THE OHIO STATE UNIVERSITY

# A Hybrid Asymptotic-Modal Analysis of the EM Scattering by an Open-Ended S-Shaped Rectangular Waveguide Cavity

P.H. Law, R.J. Burkholder and P.H. Pathak

The Ohio State University

**ElectroScience Laboratory**

Department of Electrical Engineering
Columbus, Ohio 43212

Technical Report 719630-2
Grant No. NAG3-476
December 1988

NASA Lewis Research Center
21000 Brookpark Road
Cleveland, OH 44135

## NOTICES

When Government drawings, specifications, or other data are used for any purpose other than in connection with a definitely related Government procurement operation, the United States Government thereby incurs no responsibility nor any obligation whatsoever, and the fact that the Government may have formulated, furnished, or in any way supplied the said drawings, specifications, or other data, is not to be regarded by implication or otherwise as in any manner licensing the holder or any other person or corporation, or conveying any rights or permission to manufacture, use, or sell any patented invention that may in any way be related thereto.

50272-101

| REPORT DOCUMENTATION PAGE | 1. REPORT NO. | 2. | 3. Recipient's Accession No. |
|---|---|---|---|

**4. Title and Subtitle**
A Hybrid Asymptotic-Model Analysis of the EM Scattering by an Open-Ended S-Shaped Rectangular Waveguide Cavity

**5. Report Date**
December 1988

**6.**

**7. Author(s)**
P.H. Law, R.J. Burkholder and P.H. Pathak

**8. Performing Org. Rept. No.**
719630-2

**9. Performing Organization Name and Address**
The Ohio State University
ElectroScience Laboratory
1320 Kinnear Road
Columbus, OH 43212

**10. Project/Task/Work Unit No.**

**11. Contract(C) or Grant(G) No.**
(C)
(G) NAG3-476

**12. Sponsoring Organization Name and Address**
NASA Lewis Research Center
21000 Brookpark Road
Cleveland, OH 44135

**13. Report Type/Period Covered**
Technical Report

**14.**

**15. Supplementary Notes**

**16. Abstract (Limit: 200 words)**

The EM Backscatter from a 3-dimensional perfectly conducting S-shaped open-ended cavity with a planar interior termination is analyzed when it is illuminated by an external plane wave. The analysis is based on a self-consistent multiple scattering method which accounts for the multiple wave interactions between the open end and the interior termination. The scattering matrices which described the reflection and transmission coefficients of the waveguide modes reflected and transmitted at each junction between the different waveguide sections, as well at the scattering from the edges at the open end are found via asymptotic high frequency methods such as the geometrical and physical theories of diffraction used in conjunction with the equivalent current method. The numerical results for an S-shaped inlet cavity are compared with the backscatter from a straight inlet cavity; the backscattered patterns are different because the curvature of an S-shaped inlet cavity redistributes the energy reflected from the interior termination in a way that is different from a straight inlet cavity.

**17. Document Analysis a. Descriptors**

**b. Identifiers/Open-Ended Terms**

**c. COSATI Field/Group**

| 18. Availability Statement | 19. Security Class (This Report) Unclassified | 21. No. of Pages 47 |
|---|---|---|
| | 20. Security Class (This Page) Unclassified | 22. Price |

(See ANSI-Z39.18) *See Instructions on Reverse* OPTIONAL FORM 272 (4-77)
Department of Commerce

# Contents

# List of Tables

# List of Figures

# Chapter 1

# Introduction

An analysis is developed for predicting the electromagnetic fields (EM) which are scattered from a 3-dimensional (3-D) perfectly conducting S-shaped open-ended semi-infinite waveguide cavity with a planar interior termination when it is illuminated by an external plane wave. The analysis is based on a hybrid asymptotic modal approach which has been discussed extensively in [1,2,3,4].

Briefly, this hybrid asymptotic-modal, or more simply the hybrid modal approach, models the S-shaped rectangular cavity by smoothly joining together straight and annular rectangular waveguide sections as shown in Figure 1.1. The scattering matrices which describe the reflection and transmission coefficients of the waveguide modes reflected and transmitted at each junction between the different waveguide sections, as well at the scattering from the edges at the open end are found via asymptotic high frequency approximations such as the geometrical and physical theories of diffraction used in conjunction with the equivalent current method. The multiple wave interactions between the various waveguide sections can be accounted for in a straightforward fashion, in terms of these junction scattering (reflection and transmission) matrices, via the self-consistent multiple scattering method [1,2,3,4]. It is noted that the asymptotic high frequency

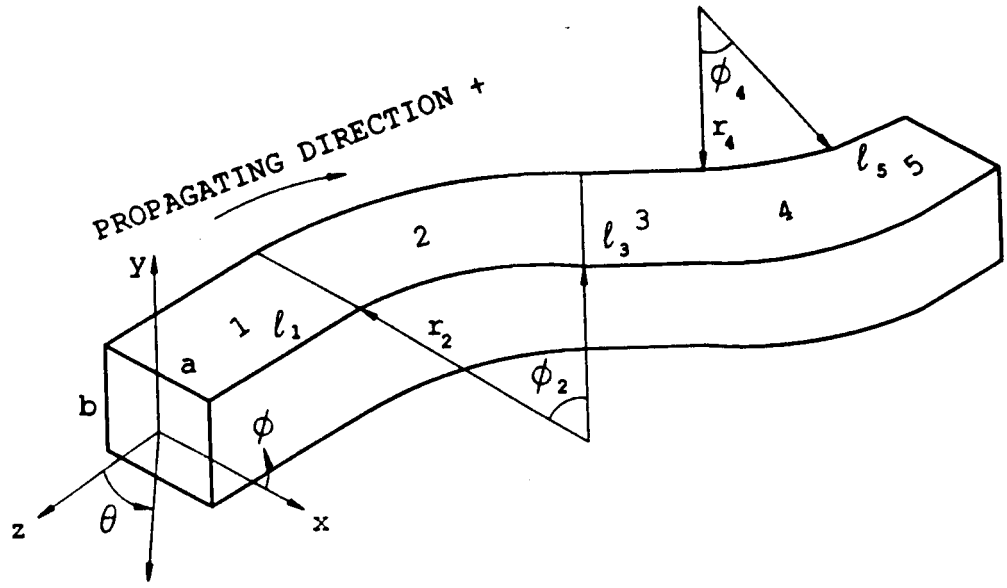


(a) oblique view

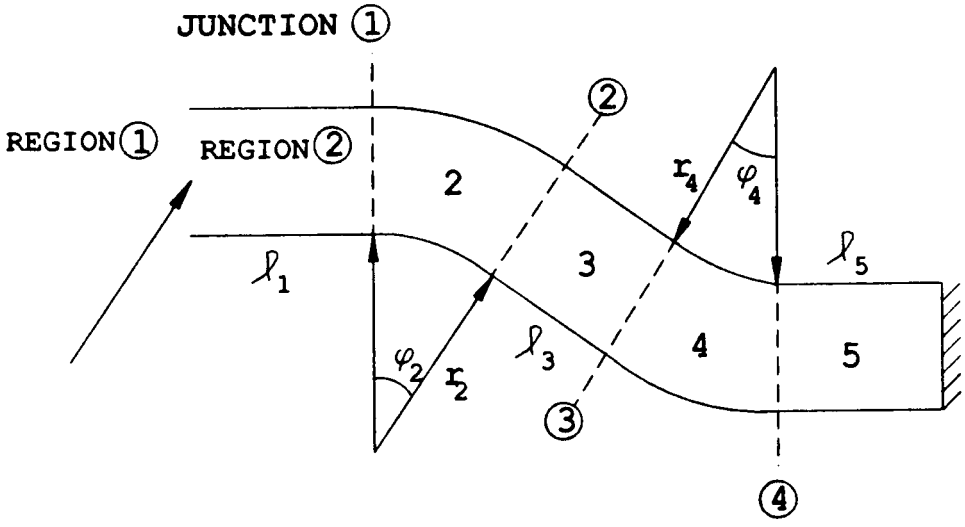


(b) top view

Figure 1.1: S-shaped cavity with rectangular cross-section formed by joining straight and annular waveguide sections.

based approach is far more efficient for calculating the modal reflection and transmission coefficient matrices for the waveguide junctions than is the classical mode matching technique, as the latter requires a numerical matrix inversion making it cumbersome and inefficient. Furthermore, these modal coefficients obtained via asymptotic high frequency approximations generally have a relatively simple form thereby lending physical insight into the modal reflection and transmission process. It is the hybrid combination of high frequency and modal techniques that makes the present approach a hybrid asymptotic-modal approach.

The modes in the straight and annular rectangular waveguide sections are known analytically, and the decomposition of these modal fields into their corresponding equivalent sets of modal rays can be performed easily. However, consistent with some previous experience [1], it is seen that the reflection coefficient matrix elements are negligible in comparison to the transmission coefficient matrix elements characterizing the smooth junctions between the straight and annular waveguide sections. Hence, it is found that the modal reflection effects can be ignored in this analysis thereby requiring one to essentially retain only the modal transmission matrix.

It is noted that in this multiple scattering method, the total scattered field consists of a superposition of three contributions, namely:

(i) contribution from the diffraction of the incident wave by the edge at the open end;

(ii) contribution from the scattering by the interior termination, which arises from part of the incident energy which couples via the open end into the S-duct (or cavity) and then reflects from the termination to partly radiate out through the open end. The remaining energy is scattered back into the cavity to again reflect from the termination, and so on. Since the reflection from the planar perfectly-conducting termination is generally

more significant than the reflection back into the cavity from the open end, the multiple wave interactions between the termination and the open end may be ignored. Also, if the reflection from the termination can be made small by making it an appropriate planar dielectric termination (say), then the interactions between the open end and the low reflection type termination can again be ignored! While the reflections of waves at each junction between the waveguide sections can contribute to the net scattering from the interior, this effect is negligible in comparison to the other effects as mentioned earlier, and it is therefore ignored making the only contribution to the scattering from the interior of the cavity as being due to the termination. Nevertheless, it is noted that any of these effects which have been ignored here can be put back directly via the multiple scattering method [1,2,3,4], if it is so desired;

(iii) contribution from the scattering by any other external features of the S-duct. This effect is not of concern to the present work and it will therefore not be included.

Since the diffraction from the open end and the modal reflection from the interior planar termination have already been found for the rectangular waveguide case, and the corresponding scattering matrices have been given explicitly for these two junctions in [2,4], it only remains to find the modal transmission coefficient scattering matrix for the junction between a straight and annular rectangular waveguide section. Before finding the latter, the general formulation for the total scattered field in terms of the multiple scattering method is first given in Chapter 2. This multiple scattering method directly employs the scattering matrix for the open end, the transmission matrices for the junction between straight and annular waveguide sections, and the reflection matrix for the planar interior termination [1,2,3,4]. The details involved in the development of the modal transmis-

sion (scattering) matrix for the junction between a straight and annular waveguide section are then presented in Chapter 3. Finally, the results for the open end and the termination scattering matrices are combined with the junction transmission scattering matrix developed in Chapter 3, in accordance with the formulation given in Chapter 2 for the total scattered field; the numerical results based on this total scattered field are presented in Chapter 4. An $e^{j\omega t}$ time convention is assumed and suppressed in the following analysis.

# Chapter 2

# Formulation Using the Self-Consistent Multiple Scattering Method

As mentioned in Chapter 1, an incident plane wave excites the fields inside the duct configuration as shown in Figure 1.1. These fields can be expanded into the natural waveguide modes of each uniform section. Transmission and reflection of waves at a junction as well as propagation through a given waveguide section are all described in terms of reflection, transmission and propagation matrices. The elements of these matrices are found using asymptotic high frequency approximations such as the geometrical and physical theories of diffraction in conjunction with the equivalent current method. The multiple wave interactions between the different junctions can be accounted for using the self-consistent Multiple Scattering Matrix (MSM) formulation [1,2,3,4] which makes use of these reflection, transmission and propagation matrices.

As a quick review of the MSM formulation, consider a a plane wave incident on an open ended parallel plate duct as shown in Figure 2(a). This 2-D scattering example is considered due to its simplicity in geometry and in formulation. The MSM result obtained can then be extended to a rectangular S-shaped duct as will be shown later in this chapter. The

scattering matrices involved in a rectangular duct are more complex than those in a parallel plate duct. Reference [2] gives a detailed discussion and derivations of these scattering matrices. For the 2-D scattering example, let the symbol $U$ be the $\hat{z}$-directed $E$-field of the TE case and the $H$-field of the TM case, respectively; this incident field can be written as

$$\vec{U}^{inc} = \hat{z}U_{inc}e^{-jk(x\cos\theta+y\sin\theta)} \tag{2.1}$$

Also, let $U^s$ refer to the field scattered into the exterior region by the waveguide cavity. Thus, $U^s$ represents the complex amplitude of the scattered electric field $\vec{E}^s = \hat{z}E^s$ for the TE case and the scattered magnetic field $\vec{H}^s = \hat{z}H^s$ for the TM case. Let

$$U^s = U_o^s + U_c^s + U_{ext}^s \tag{2.2}$$

where $U_o^s$ is the component of the field scattered into the exterior by just the edges at the open end, and $U_c^s$ is the contribution to the field scattered into the exterior through reflection from the interior termination. Also, $U_{ext}^s$ is the contribution to the scattered field due to any other external features of the duct configuration. This contribution is not of interest here and thus is neglected. In the far zone of the open end of the cavity, one can write

$$U_o^s = U_{inc}f_{e,h}(k,\theta)\frac{e^{-jkr}}{\sqrt{r}} \tag{2.3}$$

$$U_c^s = U_{inc}g_{e,h}(k,\theta)\frac{e^{-jkr}}{\sqrt{r}} \tag{2.4}$$

where $(r,\theta)$ are shown in Figure 2.1(a), and $f_{e,h}$ and $g_{e,h}$ are unknown pattern functions yet to be found.

From the self-consistent multiple scattering method [1,2,3,4], one can express the total far zone $U^s$ (minus $U_{ext}^s$) in terms of the generalized scattering matrices introduced as

$$[U^s(\vec{r})] = \left\{[S_{11}] + [S_{12}][P][\Gamma_B][P]([I] - [S_{22}][P][\Gamma_B][P])^{-1}[S_{21}]\right\}U_{inc}\frac{e^{-jkr}}{\sqrt{r}} \tag{2.5}$$

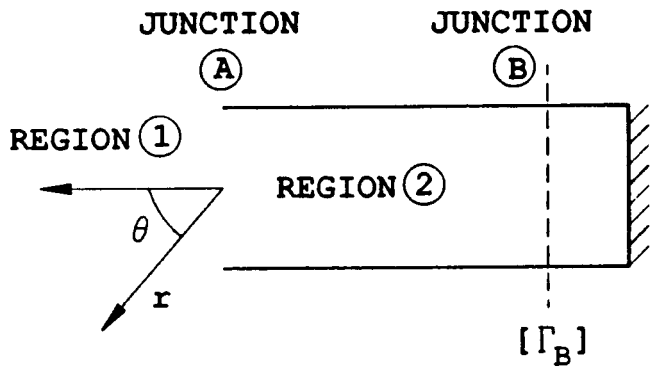


(a) parallel plate duct

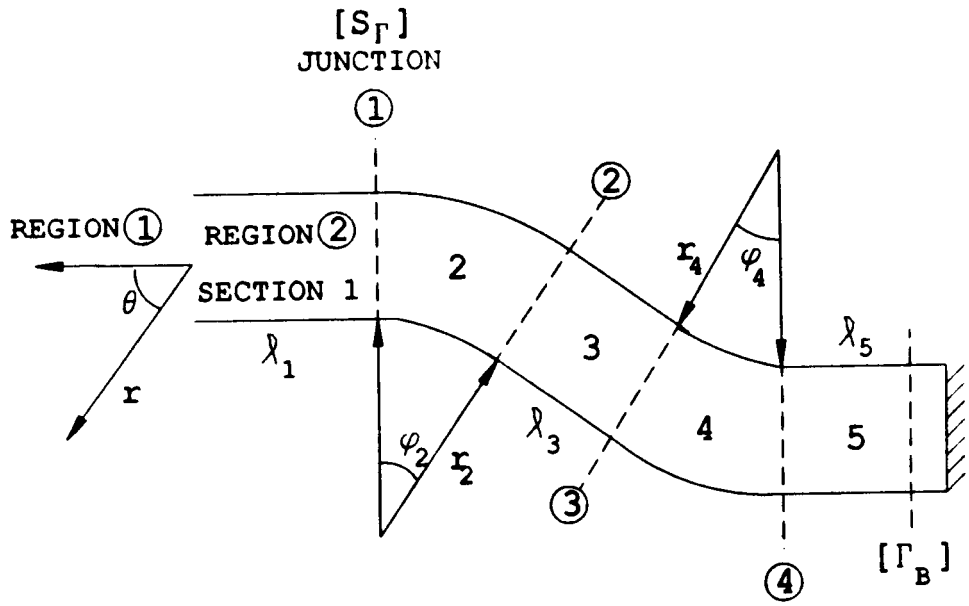


(b) 2-dimensional S-shaped duct

Figure 2.1: 2-dimensional parallel and s-shaped duct models

In (2.5), the matrix [P] denotes the phase delay of the modes as they propagate between junctions A and B; this [P] is a diagonal matrix. The $[\Gamma_B]$ in (2.5) denotes the total reflection coefficient scattering matrix at junction B which describes the modes reflected back into region 2 due to modes incident at B from region 2.

Note that if there was no termination, then $[\Gamma_B]$ would be a null matrix and the scattered field $U^s$ in (2.5) would come only from the diffraction of the incident wave at the front edges as described by $[S_{11}]$. Therefore, $[S_{11}]$ is the only scattering matrix present when there are no internal discontinuities or terminations within the cavity. From (2.3),(2.4) and (2.5), one obtains that

$$\begin{aligned} f_{e,h} &= [S_{11}] \\ &= S_{11} \end{aligned} \tag{2.6}$$

where the matrix $[S_{11}]$ has only a single element $S_{11}$; also, it follows from (2.2) that

$$g_{e,h} = [S_{12}][P][\Gamma_B][P]([I] - [S_{22}][P][\Gamma_B][P])^{-1}[S_{21}] \tag{2.7}$$

If the duct configuration is changed from a parallel plate section as shown in Figure 2.1(a) to an S-shaped duct section as shown in Figure 2.1(b), the MSM result of (2.5) is modified by simply replacing the termination reflection scattering matrix,$[\Gamma_B]$, with an effective scattering matrix, $[S_\Gamma]$. Since the front section of an S-shaped duct is a parallel plate section, it would be useful to define an effective scattering matrix, $[S_\Gamma]$, at the end of the first section to account for all of the rest of the duct sections including the final termination. The MSM results of (2.5) can then be applied to find the scattered field of an S-shaped duct in terms of this $[S_\Gamma]$. For a smoothly joined junction, it has been shown that the modal reflection coefficients are negligible compared to the modal transmission coefficients [1]. Thus the

scattering matrix,$[S_\Gamma]$ at junction 1 due to sections 2,3,4,5 can be written as:

$$[S_\Gamma] = [A]^t[\Gamma_B][A] \tag{2.8}$$

with

$$[A] = [P_5][T_{45}][P_4][T_{34}][P_3][T_{23}][P_2][T_{12}], \tag{2.9}$$

and $[A]^t$ is the transpose of $[A]$. $[A]$ is a matrix which traces the modal field structure from junction 1 to the termination. $[\Gamma_B]$ is the reflection coefficient scattering matrix due to the termination, and $[P_i]$ is the propagation phase matrix due to section $i$. $[T_{ij}]$ is the transmission matrix at the junction between sections $i$ and $j$. The subscript of $[T_{ij}]$ means propagation is from duct section $i$ to section $j$. It is also noted that $[A]$ in (2.9) gives a physical insight of how modes propagate in the duct structure. (2.9) should be read from right to left. First, the modal fields pass through a junction from section 1 to 2. The change in the modal field structure is accounted for by the modal transmission matrix $[T_{12}]$. Next, the modes propagate through section 2, and their phase delay results in a $[P_2]$. A subsequent transmission through a junction gives another transmission matrix $[T_{23}]$ and so on, until the modal fields hit the termination.

The MSM formulation in (2.5) and the effective scattering matrix in (2.8) can also be applied to a 3-dimensional S-shaped duct. In Reference [2], an analysis has been developed for predicting the near and far zone fields scattered by a rectangular waveguide terminated with a planar impedance surface. However, if one uses the effective scattering matrix $[S_\Gamma]$ due to a succession of duct sections as in (2.8) to replace the termination scattering matrix, $[\Gamma_B]$, one essentially gets the scattering patterns due to a 3-dimensional S-shaped duct just as for the 2-dimensional case described above. The solution as proposed in [2] can be used to find the scattered

field $[E^s]$ which is represented by a matrix equation as follows

$$[E^s] = \left\{[S_{11}] + [S_{12}][P][S_\Gamma][P]([I] - [S_{22}][P][S_\Gamma][P])^{-1}[S_{21}]\right\}[E^i] \tag{2.10}$$

with the scattering matrices defined as $[S_{21}]$ coupling matrix from an external source to modal excitations,

$[S_{12}]$ radiation matrix from modal fields to an external field point,

$[S_{22}]$ internal reflection matrix at the waveguide aperture,

$[P]$ the modal propagation phase delay matrix,

$[E^i]$ incident field of the external source, and

$[S_\Gamma]$ the effective reflection matrix at the end of the first section.

All these matrices are well defined in [2] except the effective scattering matrix $[S_\Gamma]$ which is defined in Equations (2.8) and (2.9). The transmission matrix, $[T_{ij}]$ as appeared in (2.9), will be discussed in the next chapter. $[E^s]$ and $[E^i]$ are column matrices with three elements representing the three vector components of $\vec{E}^s$ and $\vec{E}^i$, respectively. Once $[S_\Gamma]$ is found, Equation (2.10) can be used to simulate farfield patterns which will be the topic of Chapter 4.

# Chapter 3

# Modal Transmission Coefficient for the Junction Between a Straight and an Annular Rectangular Waveguide Section

To determine the junction transmission matrix, the modal fields of the straight and annular rectangular waveguides must be defined first; this is done in sections 3.1 and 3.2. The junction scattering matrix is then given in 3.3.

## 3.1 Modal Field Structure of a Straight Rectangular Waveguide

Figure 3.1 shows the geometry of the straight rectangular duct section. The modal electric field $\vec{E}^{r\pm}$ within this straight rectangular waveguide region ($z < 0$) may be represented in the usual manner [1,2,3,4] as:

$$\vec{E}^{r\pm} = \sum_n \sum_m \left[ A^{r\pm}_{nm} \vec{e}^{\,r'}_{nm} e^{\mp j\beta^{r'}_{nm} z} + B^{r\pm}_{nm} \left( \vec{e}^{\,r}_{nm} \pm \hat{z} e^{r}_{znm} \right) e^{\mp j\beta^{r}_{nm} z} \right]. \quad (3.1)$$

Here, $\vec{e}^{\,r'}_{nm}$ and $\vec{e}^{\,r}_{nm}$ denote the transverse (to $z$) electric vector mode functions for the $TE_{nm}$ and $TM_{nm}$ modes, respectively (where $TE$ and $TM$

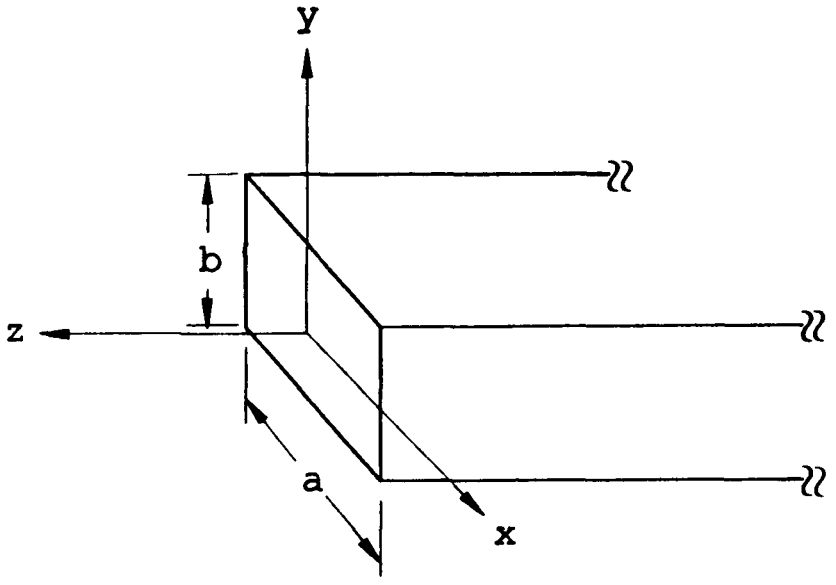


Figure 3.1: Geometry of the straight rectangular waveguide section.

are with respect to the $\hat{z}$-direction). Likewise, the $\beta^{r'}_{nm}$ and $\beta^{r}_{nm}$ denote the propagating constants of the $TE_{nm}$ and $TM_{nm}$ modes, respectively. It is noted that $e^{r}_{znm}$ is the $\hat{z}$-component of the $TM_{nm}$ modal electric field. The superscripts $+$ and $-$ in Equation (3.1) refer to modes propagating in the $+\hat{z}$ and $-\hat{z}$ directions, and the superscript $r$ implies that the fields pertain to a straight rectangular waveguide section. It is also convenient to define the magnetic field $\vec{H}^{r\pm}$ in the straight rectangular waveguide region following the representation for the electric field $\hat{E}^{r\pm}$ in (3.1); thus

$$\vec{H}^{r\pm} = \sum_n \sum_m \left[ A^{r\pm}_{nm} \left( \pm \bar{h}^{r'}_{nm} + \hat{z} h^{r'}_{znm} \right) e^{\mp j\beta^{r'}_{nm} z} + B^{r\pm}_{nm} \left( \pm \bar{h}^{r}_{nm} \right) e^{\mp j\beta^{r}_{nm} z} \right]. \tag{3.2}$$

The $A^{r\pm}_{nm}$ and $B^{r\pm}_{nm}$ in (3.1) and (3.2) are the modal coefficients which can be determined once the excitation is known. The $\bar{h}^{r'}_{nm}$ and $\hat{z}h^{r'}_{znm}$ are the magnetic vector mode functions for the $TE_{nm}$ modes, whereas $\bar{h}^{r'}_{nm}$ is the magnetic vector mode function for the $TM_{nm}$ modes. Table 3.1 gives the explicit forms of the propagating mode functions in a straight rectangular waveguide. For the derivation and explicit expressions for these modes, one

can refer to a well known text such as [5].

## 3.2 Modal Field Structure of an Annular Duct

The modal fields for an annular duct also of rectangular cross-section, which is shown in Figure 3.2, can be established in a similar manner. Now, since the propagation is along the $\pm\hat{\phi}$ directions, and $\hat{\phi}$ is not a constant vector, the fields $\vec{E}^{a\pm}$ and $\vec{H}^{a\pm}$ are initially defined as having components transverse to $\hat{z}$ and along $\hat{z}$, respectively. Afterwards, these modal fields can be rearranged to give a more convenient set of modes; i.e., transverse to $\hat{\phi}$ and axial to $\hat{\phi}$, since $\hat{\phi}$ is the propagating direction. The modal electric field $\vec{E}^{a\pm}$ and the magnetic field $\vec{H}^{a\pm}$ can then be written as:

$$\vec{E}^{a\pm} = \sum_p \sum_q \left[ C_{pq}^{a\pm} \left( \bar{e}_{pq}^{a\prime} \pm \hat{\phi} e_{\phi pq}^{a\prime} \right) e^{\mp j\nu_{pq}^{a\prime}\phi} + D_{pq}^{a\pm} \left( \bar{e}_{pq}^{a} \pm \hat{\phi} e_{\phi pq}^{a} \right) e^{\mp j\nu_{pq}^{a}\phi} \right] \tag{3.3}$$

$$\vec{H}^{a\pm} = \sum_p \sum_q \left[ C_{pq}^{a\pm} \left( \pm \bar{h}_{pq}^{a\prime} + \hat{\phi} h_{\phi pq}^{a\prime} \right) e^{\mp j\nu_{pq}^{a\prime}\phi} + D_{pq}^{a\pm} \left( \pm \bar{h}_{pq}^{a} + \hat{\phi} h_{\phi pq}^{a} \right) e^{\mp j\nu_{pq}^{a}\phi} \right] \tag{3.4}$$

Again, $\bar{e}_{pq}^{a\prime}$ and $\bar{e}_{pq}^{a}$ denote the transverse (to $\phi$) electric vector mode functions for the $TE_{pq}$ and $TM_{pq}$ modes ,and the $\bar{h}_{pq}^{a\prime}$ and $\bar{h}_{pq}^{a}$ denote the transverse (to $\phi$) magnetic vector mode functions for the $TE_{pq}$ and $TM_{pq}$, respectively. The superscript a implies that the fields pertain in the annular duct section. The modal field structure of an annular duct will be discussed in more detail in the next section.

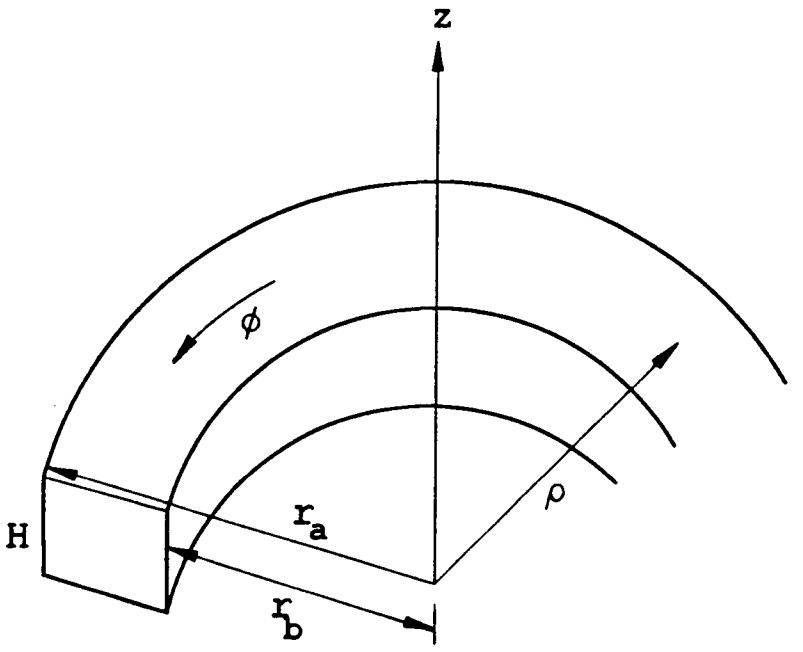


Figure 3.2: Geometry of the annular waveguide section.

### 3.2.1 Modal Field Structure Calculations

In an annular waveguide (as shown in Figure 3.2), there are always a finite number of propagating modes. These modes can be classified into sets of $TM$ to $z$ or $TE$ to $z$, where the former set of modes has no $H_z$ field and the latter set of modes has no $E_z$ field. A combination of these two sets of modes gives a complete field structure inside the waveguide. In addition to these propagating modes, there are also an infinite number of evanescent modes. These evanescent modes decay exponentially along the waveguide axis. For the present analysis, the effects of these evanescent modes are ignored.

**$TM$ (transverse to $z$) modes:**

The $TM_z$ fields can be found via a $\hat{z}$-directed magnetic vector potential, $\vec{A} = \Psi\hat{z}$. The magnetic vector potential satisfies the wave equation

$$\left(\nabla^2 + k^2\right)\vec{A} \;=\; 0 \tag{3.5}$$

where $k$ is the free space wave number, $2\pi/\lambda$. But, since $\hat{z}$ is a constant vector, the above equation can be reduced to a scalar form as:

$$\left(\nabla^2 + k^2\right)\Psi = 0. \tag{3.6}$$

This equation in cylindrical coordinates can be rewritten as:

$$\left[\frac{1}{\rho}\frac{\partial}{\partial\rho}\left(\rho\frac{\partial}{\partial\rho}\right) + \frac{1}{\rho^2}\frac{\partial^2}{\partial\phi^2} + \frac{\partial^2}{\partial z^2} + k^2\right]\Psi = 0. \tag{3.7}$$

The electric and magnetic fields are related to $\Psi$ as [6]:

$$\begin{cases} E_\rho = \frac{Z_o}{jk}\frac{\partial^2\Psi}{\partial\rho\partial z} & H_\rho = \frac{1}{\rho}\frac{\partial\Psi}{\partial\phi} \\ E_\phi = \frac{Z_o}{jk}\frac{1}{\rho}\frac{\partial^2\Psi}{\partial\phi\partial z} & H_\phi = -\frac{\partial\Psi}{\partial\rho} \\ E_z = \frac{Z_o}{jk}\left(\frac{\partial^2}{\partial z^2} + k^2\right)\Psi & H_z = 0. \end{cases} \tag{3.8}$$

The boundary conditions used to find $\Psi$ are that all tangential electric field components are zero on the walls of the guide. In order to construct $\Psi$, let the separation of variables suggest a solution of the form:

$$\Psi(\rho,\phi,z) = R(\rho)\Phi(\phi)Z(z). \tag{3.9}$$

Substituting Equation (3.9) into Equation (3.7) and introducing two separation constants $p_1$ and $\nu_q$, one will get three differential equations as follows:

$$\frac{1}{Z}\frac{\partial^2}{\partial z^2}Z = -p_1^2 \tag{3.10}$$

$$\frac{1}{\Phi}\frac{\partial^2\Phi}{\partial\phi^2} = -\nu_q^2 \tag{3.11}$$

$$\rho\frac{\partial}{\partial\rho}\left(\rho\frac{\partial R}{\partial\rho}\right) + \left[\left(k^2 - p_1^2\right)\rho^2 - \nu_q^2\right]R = 0. \tag{3.12}$$

The solutions to Equation (3.11) are

$$\Phi(\phi) = e^{-j\nu_q\phi} \text{ and } e^{+j\nu_q\phi} \tag{3.13}$$

where modes propagate in the $\pm\hat{\phi}$ directions.

The solution to Equation (3.10) is

$$Z(z) \;=\; A\cos p_1 z + B\sin p_1 z. \tag{3.14}$$

Since $E_\phi = \frac{Z_o}{jk}\frac{1}{\rho}\frac{\partial^2\Psi}{\partial\phi\partial z}$, the boundary condition

$$E_\phi(z=0; z=l) \;=\; 0 \tag{3.15}$$

implies

$$\frac{\partial Z}{\partial z}(z=0; z=l) \;=\; 0. \tag{3.16}$$

Therefore, from (3.14) and (3.16), $B = 0$ and $p_1 = \frac{p\pi}{l}$. Hence, $Z(z)$ can be rewritten as

$$Z(z) \;=\; A\cos\frac{p\pi}{l}z,\; p = 0, 1, \cdots \tag{3.17}$$

Likewise, (3.12) is a Bessel's equation and has solutions $R(\rho)$ which can be linear combinations of $H^{(1)}_{\nu_q}(k_c\rho)$ and $H^{(2)}_{\nu_q}(k_c\rho)$ with

$$k_c \;=\; \sqrt{k^2 - \left(\frac{p\pi}{l}\right)^2} \tag{3.18}$$

where $H^{(1)}_{\nu_q}(k_c\rho)$ and $H^{(2)}_{\nu_q}(k_c\rho)$ are Hankel functions of the first and second kinds, respectively, of order $\nu_q$ and argument $k_c\rho$. From the boundary condition on the $\hat{z}$ directed $\vec{E}$ field, one obtains

$$E_z(\rho=a; \rho=b) \;=\; 0. \tag{3.19}$$

Next, one can utilize (3.19) and (3.8) to obtain

$$\begin{aligned} E_z \;&=\; \frac{Z_o}{jk}\left[k^2 + \frac{\partial^2}{\partial z^2}\right]\Psi \\ &=\; \frac{Z_o}{jk}\left[k^2 - \left(\frac{p\pi}{l}\right)^2\right]\Psi(\rho=a; \rho=b) = 0. \end{aligned} \tag{3.20}$$

Now $R(\rho)$ can be constructed via (3.20) as

$$R(\rho) \;=\; \frac{1}{2j}\left[H^{(2)}_{\nu_q}(k_c b)H^{(1)}_{\nu_q}(k_c\rho) - H^{(1)}_{\nu_q}(k_c b)H^{(2)}_{\nu_q}(k_c\rho)\right]. \tag{3.21}$$

Note that $R(b) = 0$ has been employed. To satisfy $\Psi(\rho = a) = 0$, the eigenvalues $\nu_q$ can be found numerically by solving the equation

$$R(a) = 0. \tag{3.22}$$

Since $R(\rho)$ in (3.21) depends on $p$ and $q$, $R(\rho)$ should be rewritten as $R_{pq}(\rho)$. Consequently, the eigenvalues $\nu_q$ found from (3.22) should be dependent on $p$ and hence are renamed as $\nu_{pq}$.

Using linear combinations of these solutions and enforcing the boundary conditions gives the complete solution for the magnetic potential $\Psi$ which can be written as

$$\Psi = \sum_{p=0}\sum_{q=1} C^{+}_{pq} R_{pq}(\rho)\cos\left(\frac{p\pi}{l}z\right) e^{-j\nu_{pq}\phi} + C^{-}_{pq} R_{pq}(\rho)\cos\left(\frac{p\pi}{l}z\right) e^{j\nu_{pq}\phi} \tag{3.23}$$

where $C^{\pm}_{pq}$ is related to the modal coefficients.

The electric and magnetic fields inside the waveguide thus can be found from Equation (3.8). In addition, these modal fields can be put in a form to fit Equations (3.3) and (3.4). For example, the $TM_{pq}$ electric modal field $\vec{E}^{a\pm}_{e}$ can be written as:

$$\vec{E}^{a\pm}_{e} = \left(\bar{e}^{a}_{pq} \pm \hat{\phi} e^{a}_{\phi pq}\right) e^{\mp j\nu^{a}_{pq}\phi}. \tag{3.24}$$

The subscript $e$ means the field is $TM$ or $e$ type. Also by definition $\bar{e}^{a}_{pq}$ are field components transverse to $\phi$, thus from (3.8) one gets

$$\begin{cases} \bar{e}^{a}_{pq} e^{\mp j\nu^{a}_{pq}\phi} = \hat{z} E^{e\pm}_{zpq} + \hat{\rho} E^{e\pm}_{\rho pq} \\ \hat{\phi} e^{a}_{\phi pq} e^{\mp j\nu^{a}_{pq}\phi} = \hat{\phi} E^{e\pm}_{\phi pq}. \end{cases} \tag{3.25}$$

$E^{e\pm}_{zpq}$, $E^{e\pm}_{\rho pq}$ and $E^{e\pm}_{\phi pq}$ are found from (3.8) and (3.23) which are summarized in (3.28-3.30).

The $TM_{pq}$ magnetic modal field $\vec{H}^{a\pm}_{e}$ can be put in a similar form, from Equation (3.4):

$$\vec{H}^{a\pm}_{e} = \left(\pm \bar{h}^{a}_{pq} + \hat{\phi} h^{a}_{\phi pq}\right) e^{\mp j\nu^{a}_{pq}\phi}. \tag{3.26}$$

where

$$\begin{cases} \bar{h}^a_{pq} e^{\mp j\nu^a_{pq}\phi} &= \hat{\rho} H^{e\pm}_{\rho pq} \\ \hat{\phi} h^a_{\phi pq} e^{\mp j\nu^a_{pq}\phi} &= \hat{\phi} H^{e\pm}_{\phi pq}. \end{cases} \tag{3.27}$$

The individual electric and magnetic field components can be summarized as follows:

$$E^{e\pm}_{\rho pq} = A_{pq} \frac{Z_o}{k} \left(\frac{p\pi}{l}\right) \sin\left(\frac{p\pi}{l} z\right) R'_{pq}(\rho) e^{\mp j\nu_{pq}\phi} \tag{3.28}$$

$$E^{e\pm}_{\phi pq} = -A_{pq} \frac{j Z_o \nu_{pq}}{k\rho} \left(\frac{p\pi}{l}\right) \sin\left(\frac{p\pi}{l} z\right) R_{pq}(\rho) e^{\mp j\nu_{pq}\phi} \tag{3.29}$$

$$E^{e\pm}_{zpq} = -A_{pq} \frac{Z_o}{k} \left[k^2 - \left(\frac{p\pi}{l}\right)\right] \cos\left(\frac{p\pi}{l} z\right) R_{pq}(\rho) e^{\mp j\nu_{pq}\phi} \tag{3.30}$$

$$H^{e\pm}_{\rho pq} = -A_{pq} \frac{\nu_{pq}}{\rho} \cos\left(\frac{p\pi}{l} z\right) R_{pq}(\rho) e^{\mp j\nu_{pq}\phi} \tag{3.31}$$

$$H^{e\pm}_{\phi pq} = A_{pq} j \cos\left(\frac{p\pi}{l} z\right) R'_{pq}(\rho) e^{\mp j\nu_{pq}\phi} \tag{3.32}$$

$$H^{e\pm}_{zpq} = 0. \tag{3.33}$$

The normalization constant $A_{pq}$ is found by normalizing the power carried by the $pq^{th}$ mode to unity. This is done by integrating the Poynting vector over a cross section of the guide and setting this equal to unity,

$$\int\int_S \left(\bar{e}^a_{pq} \times \bar{h}^a_{pq}\right) \cdot \hat{\phi} dS = 1. \tag{3.34}$$

Substituting (3.25) and (3.27) into (3.34), $A_{pq}$ can be found as

$$A_{pq} = \left\{ \frac{Z_o \varepsilon l}{2k} \nu_{pq} \left[k^2 - \left(\frac{p\pi}{l}\right)^2\right] \int_b^a \frac{R^2_{pq}(\rho)}{\rho} d\rho \right\}^{-\frac{1}{2}} \tag{3.35}$$

where

$$\varepsilon = \begin{cases} 2 & , p = 0 \\ 1 & , p \neq 0. \end{cases} \tag{3.36}$$

**$TE$ (transverse to $z$) modes:**

The derivation for the $TE_{pq}$ fields is very similar to that for the $TM_{pq}$ fields. They can be found as follows:

Let $\vec{F} = \Psi \hat{z}$ be the electric vector potential satisfying the wave equation

$$\left(\nabla^2 + k^2\right) \vec{F} \;=\; 0 \tag{3.37}$$

which can be reduced to a scalar form as in Equation (3.6). The electric and magnetic fields are related to this potential as [6]

$$\begin{cases} E_\rho = -\frac{1}{\rho}\frac{\partial \Psi}{\partial \phi} & H_\rho = \frac{1}{jkZ_o}\frac{\partial^2 \Psi}{\partial \rho \partial z} \\ E_\phi = \frac{\partial \Psi}{\partial \rho} & H_\phi = \frac{1}{jkZ_o}\frac{1}{\rho}\frac{\partial^2 \Psi}{\partial \phi \partial z} \\ E_z = 0 & H_z = \frac{1}{jkZ_o}\left(\frac{\partial^2}{\partial z^2} + k^2\right)\Psi. \end{cases} \tag{3.38}$$

Again, using the boundary conditions that electric field components are zero on the walls, these field components can be put in a form as in Equations (3.3) and (3.4), such that

$$\vec{E}_h^{a\pm} \;=\; \left(\bar{e}_{pq}^{a'} \pm \hat{\phi} e_{\phi pq}^{a'}\right) e^{\mp j \nu_{pq}^{a'} \phi}, \tag{3.39}$$

and from (3.38) one gets:

$$\begin{cases} \bar{e}_{pq}^{a'} e^{\mp j \nu_{pq}^{a'} \phi} &= \hat{\rho} E_{\rho pq}^{h\pm} \\ \hat{\phi} e_{\phi pq}^{a'} e^{\mp j \nu_{pq}^{a'} \phi} &= \hat{\phi} E_{\phi pq}^{h\pm}. \end{cases} \tag{3.40}$$

The subscript $h$ in (3.39) and the same superscript in (3.40) means the field is $TE$ or $h$ type. Furthermore, $E_{\rho pq}^{h\pm}$ and $E_{\phi pq}^{h\pm}$ are summarized in (3.43) and (3.44), respectively. It is similar for the $TE_{pq}$ case

$$\vec{H}_h^{a\pm} \;=\; \left(\pm \bar{h}_{pq}^{a'} + \hat{\phi} h_{\phi pq}^{a'}\right) e^{\mp j \nu_{pq}^{a'} \phi} \tag{3.41}$$

where

$$\begin{cases} \bar{h}_{pq}^{a'} e^{\mp j \nu_{pq}^{a'} \phi} &= \hat{z} H_{zpq}^{h\pm} + \hat{\rho} H_{\rho pq}^{h\pm} \\ \hat{\phi} h_{\phi pq}^{a'} e^{\mp j \nu_{pq}^{a'} \phi} &= \hat{\phi} H_{\phi pq}^{h\pm}. \end{cases} \tag{3.42}$$

The individual field components can be summarized as follows:

$$E_{\rho pq}^{h\pm} \;=\; B_{pq} \frac{\nu_{pq}}{\rho} \sin\left(\frac{p\pi}{l} z\right) R_{pq}(\rho) e^{\mp j \nu_{pq} \phi} \tag{3.43}$$

$$E^{h\pm}_{\phi pq} = -B_{pq} j \sin\left(\frac{p\pi}{l}z\right) R'_{pq}(\rho) e^{\mp j\nu_{pq}\phi} \quad (3.44)$$

$$E^{h\pm}_{zpq} = 0 \quad (3.45)$$

$$H^{h\pm}_{\rho pq} = -B_{pq}\frac{1}{kZ_o}\left(\frac{p\pi}{l}\right)\cos\left(\frac{p\pi}{l}z\right) R'_{pq}(\rho) e^{\mp j\nu_{pq}\phi} \quad (3.46)$$

$$H^{h\pm}_{\phi pq} = B_{pq}\frac{j}{Z_o k\rho}\left(\frac{p\pi}{l}\right)\cos\left(\frac{p\pi}{l}z\right) R_{pq}(\rho) e^{\mp j\nu_{pq}\phi} \quad (3.47)$$

$$H^{h\pm}_{zpq} = -B_{pq}\frac{1}{kZ_o}\left[k^2 - \left(\frac{p\pi}{l}\right)^2\right]\sin\left(\frac{p\pi}{l}z\right) R_{pq}(\rho) e^{\mp j\nu_{pq}\phi} \quad (3.48)$$

where

$$R_{pq}(\rho) = \frac{1}{2j}\left[H^{(2)\prime}_{\nu_{pq}}(k_c b) H^{(1)}_{\nu_{pq}}(k_c\rho) - H^{(1)\prime}_{\nu_{pq}}(k_c b) H^{(2)}_{\nu_{pq}}(k_c\rho)\right] \quad (3.49)$$

$$k_c = \sqrt{k^2 - \left(\frac{p\pi}{l}\right)^2}. \quad (3.50)$$

The normalizing constant, $B_{pq}$, is

$$B_{pq} = \left\{\frac{l}{2kZ_o}\nu_{pq}\left[k^2 - \left(\frac{p\pi}{l}\right)^2\right]\int_b^a \frac{R^2_{pq}(\rho)}{\rho} d\rho\right\}^{-\frac{1}{2}} \quad (3.51)$$

with $R_{pq}(\rho)$ defined in (3.49).

## 3.3 Junction Transmission Matrix

In this section, the junction transmission matrix from a rectangular waveguide to an annular waveguide is discussed. When the modal fields are transmitted from a rectangular duct section to an annular duct section, the field representation must be transformed from rectangular modes to annular modes. Since both of these modal field structures are well-defined, the question left is to find the suitable excitation coefficients for the transmitted annular modes. A junction transmission matrix performs this function; it finds the annular transmitted fields once the incident rectangular modal fields are known. This transmission matrix is obtained by employing the incident modal fields to define the equivalent surface current at the junction aperture. The latter equivalent sources then generate the transmitted annular fields.

It is noted that the modal coefficients $A_{nm}^{r\pm}$ and $B_{nm}^{r\pm}$ for the straight rectangular guide as in (3.1-2), and $C_{pq}^{a\pm}$ together with $D_{pq}^{a\pm}$ for the annular guide as in (3.3-4) can be represented as column vectors by

$$TE \text{ Rectangular Guide Modes:} \quad [A_{nm}^{r\pm}] = \begin{bmatrix} A_{11}^{r\pm} \\ \vdots \\ A_{NM}^{r\pm} \end{bmatrix} \tag{3.52}$$

$$TM \text{ Rectangular Guide Modes:} \quad [B_{nm}^{r\pm}] = \begin{bmatrix} B_{11}^{r\pm} \\ \vdots \\ B_{NM}^{r\pm} \end{bmatrix} \tag{3.53}$$

$$TE \text{ Annular Guide Modes:} \quad [C_{pq}^{a\pm}] = \begin{bmatrix} C_{11}^{a\pm} \\ \vdots \\ C_{PQ}^{a\pm} \end{bmatrix} \tag{3.54}$$

$$TM \text{ Annular Guide Modes:} \quad [D_{pq}^{a\pm}] = \begin{bmatrix} D_{11}^{a\pm} \\ \vdots \\ D_{PQ}^{a\pm} \end{bmatrix} \tag{3.55}$$

If the rectangular modal fields are incident on a rectangular/annular duct junction, the modal coefficients for the transmitted fields in the annular re-

gion are related to the incident modal coefficients by a transmission matrix, $T_{12}$, as

$$\begin{bmatrix} [C^{a+}_{pq}] \\ [D^{a+}_{pq}] \end{bmatrix} = \underbrace{\begin{bmatrix} [\Gamma^{hh}_{pq;nm}] & [\Gamma^{he}_{pq;nm}] \\ [\Gamma^{eh}_{pq;nm}] & [\Gamma^{ee}_{pq;nm}] \end{bmatrix}}_{[T_{12}]} \begin{bmatrix} [A^{r+}_{nm}] \\ [B^{r+}_{nm}] \end{bmatrix} \tag{3.56}$$

where the subscript of $[T_{12}]$ means propagation is from duct section 1 to duct section 2. In this case, section 1 is a straight rectangular section and section 2 is an annular duct section. Futhermore, the meaning of $\Gamma^{he}_{pq;nm}$ is the following. A rectangular $TM_{nm}$ (or e type) mode with modal amplitude $B^{r+}_{nm}$ which is incident at the junction is partly transformed into an annular $TE_{pq}$ (or h type) mode with modal amplitude as

$$C^{a+}_{pq} = \Gamma^{he}_{pq;nm} B^{r+}_{nm} \tag{3.57}$$

and the rest is transformed into an annular $TM_{pq}$ mode with modal coefficient $D^{a+}_{pq}$. The + sign in the above equation defines the propagating direction towards the termination as indicated in Figure 1.1. When propagation reverses direction, the modal fields from an annular duct would be incident on the junction. The new transmission matrix $[T_{21}]$ can be shown by reciprocity to be the transpose of the transmission matrix $[T_{12}]$. This relationship can be written as:

$$[T_{21}] = [T_{12}]^t \tag{3.58}$$

where t is a transpose operator.

The junction transmission matrix $[T_{12}]$ as shown in Equation (3.56) has four submatrices. Each of these submatrices carries a different function. For example, the submatrix $[\Gamma^{he}_{pq;nm}]$ transforms the incident $TM_{nm}$ rectangular modes into the transmitted $TE_{pq}$ annular modes. These submatrix elements can be found by employing the incident modal fields to define

equivalent incident electric and magnetic surface currents in the aperture formed by the junction via the Kirchhoff approximation and then evaluating the amplitudes of the transmitted modes which are produced by those equivalent currents as follows [1,2]:

$$B_{pq}^{at} = -\frac{1}{2}\left[\int\int_S \left(\vec{E}_{pq}^{a+} \cdot \vec{J} - \vec{H}_{pq}^{a+} \cdot \vec{M}\right) dS\right] \tag{3.59}$$

where $B_{pq}^{at}$ is the transmitted modal excitation which is $C_{pq}^{a+}$ or $D_{pq}^{a+}$ for $TE_{pq}$ or $TM_{pq}$ transmitted, respectively. $\vec{E}_{pq}^{a+}$ and $\vec{H}_{pq}^{a+}$ are the transmitted modal fields which can be represented by Equations (3.28) to (3.33) for $TM_{pq}$ transmitted and by Equations (3.43) to (3.48) for $TE_{pq}$ transmitted. These fields can be expressed as

for $TM_{pq}$ transmitted:

$$\begin{aligned} \vec{E}_{pq}^{a+} &= \bar{e}_{pq}^{a} + \hat{\phi} e_{\phi pq}^{a} \\ &= \hat{z} E_{zpq}^{e+} + \hat{\rho} E_{\rho pq}^{e+} + \hat{\phi} E_{\phi pq}^{e+} \end{aligned} \tag{3.60}$$

$$\begin{aligned} \vec{H}_{pq}^{a+} &= \bar{h}_{pq}^{a} + \hat{\phi} h_{\phi pq}^{a} \\ &= \hat{\rho} H_{\rho pq}^{e+} + \hat{\phi} H_{\phi pq}^{e+} \end{aligned} \tag{3.61}$$

and for $TE_{pq}$ transmitted:

$$\begin{aligned} \vec{E}_{pq}^{a+} &= \bar{e}_{pq}^{a'} + \hat{\phi} e_{\phi pq}^{a'} \\ &= \hat{\rho} E_{\rho pq}^{h+} + \hat{\phi} E_{\phi pq}^{h+} \end{aligned} \tag{3.62}$$

$$\begin{aligned} \vec{H}_{pq}^{a+} &= \bar{h}_{pq}^{a'} + \hat{\phi} h_{\phi pq}^{a'} \\ &= \hat{z} H_{zpq}^{h+} + \hat{\rho} H_{\rho pq}^{h+} + \hat{\phi} H_{\phi pq}^{h+}. \end{aligned} \tag{3.63}$$

Note that the phase factor $e^{-j\nu_{pq}\phi}$ has been suppressed because its effect will be included later in the propagating modal phase path delay matrix $[P]$. Furthermore the expressions for the annular modal fields components $E_{zpq}^{+}$, $E_{\rho pq}^{+}$, $E_{\phi pq}^{+}$, $H_{zpq}^{+}$, $H_{\rho pq}^{+}$ and $H_{\phi pq}^{+}$ are summarized in Equations (3.28) to (3.33) for the $TM$ case and in Equations (3.43) to (3.48) for the $TE$

case. $\vec{J}$ and $\vec{M}$ in (3.59) are the equivalent incident electric and magnetic currents, respectively. They can be written as

$$\vec{J} = \hat{n} \times \vec{H} \tag{3.64}$$

$$\vec{M} = \vec{E} \times \hat{n} \tag{3.65}$$

where $\hat{n}$ is the unit aperture normal vector pointing in the direction of propagation of the incident modal field. The $\vec{E}$ and $\vec{H}$ in (3.64) and (3.65) are found via the Kirchhoff method as mentioned earlier; hence, $\vec{E}$ and $\vec{H}$ are assumed to be given by the $TM$ and $TE$ incident fields as follows:

(1) for $TM_{nm}$ incident:

$$\vec{E} = \bar{e}^{r}_{nm} - \hat{z} e^{r}_{znm} \tag{3.66}$$

$$\vec{H} = -\bar{h}^{r}_{nm} \tag{3.67}$$

and (2) for $TE_{nm}$ incident:

$$\vec{E} = \bar{e}^{r'}_{nm} \tag{3.68}$$

$$\vec{H} = -\bar{h}^{r'}_{nm} + \hat{z} h^{r'}_{znm}. \tag{3.69}$$

The field components for both the $TE_{nm}$ and $TM_{nm}$ cases are summarized in Table 3.1.

Each of the four submatrices can be represented by a combination of two sets of Equations. The first set of equations is chosen either from (3.60) and (3.61) for the transmitted annular $TM_{pq}$ fields or from (3.62) and (3.63) for the transmitted annular $TE_{pq}$ fields. The second set of equations comprises either of (3.66) and (3.67) for the incident rectangular $TM_{nm}$ mode or of (3.68) and (3.69) for the incident rectangular $TE_{nm}$ mode. For example, substituting the first set of Equations (3.60), (3.61) and the second set (3.68), (3.69) into Equation (3.59), one gets the transmission submatrix $\Gamma^{eh}_{pq;nm}$ which transforms a rectangular $TE_{nm}$ mode into an annular $TM_{pq}$

mode. The four possible combinations of these two sets of equations generate the four submatrices in the transmission matrix. The formulations for these submatrices are summarized in Table 3.2.

There is one junction transmission matrix for each junction in the duct structure as shown in Figure 1.1. However some of the junction matrices are equal due to symmetry. These relationships are as follows:

$$[T_{12}] = [T_{32}] = [T_{23}]^t \tag{3.70}$$

and, if $r_2 = r_4$ in Figure 1.1, then

$$[T_{12}] = [T_{54}] = [T_{45}]^t. \tag{3.71}$$

There is a reversal of coordinate systems at the junctions between sections 3 and 4. Therefore, $[T_{45}] \neq [T_{43}]$. However, it can be shown that there is a simple relationship between the elements of the matrices $[T_{12}]$ and $[T_{34}]$. For both the rectangular $TE$ and $TM$ cases, this relationship is given by

$$[T_{34}]^{nm} = -(-1)^n [T_{12}]^{nm} \tag{3.72}$$

where $nm$ is the rectangular mode number in the width ($x$-direction) and in the height ($y$-direction) dimensions, respectively. Due to the symmetry relations of the transmission matrices, if the inner radius of the curved sections are equal, i.e., $r_2 = r_4$, then only $[T_{12}]$ is needed to be evaluated in order to find $[A]$ in (2.9).

Table 3.1: Properties of Modes in Rectangular Waveguide

| | $TE_{nm}$ | $TM_{nm}$ |
|---|---|---|
| $h_z$ | $= n_{nm} Y_{nm} \frac{n_a^2+m_b^2}{j\beta_{nm}} \cos n_a x \cos m_b y$ | $0$ |
| $e_z$ | $= 0$ | $-N_{nm} \frac{n_a^2+m_b^2}{j\beta_{nm}} \sin n_a x \sin m_b y$ |
| $h_x$ | $= N_{nm} Y_{nm} n_a \sin n_a x \cos m_b y$ | $-N_{nm} Y_{nm} m_b \sin n_a x \cos m_b y$ |
| $h_y$ | $= N_{nm} Y_{nm} m_b \cos n_a x \sin m_b y$ | $N_{nm} Y_{nm} n_a \cos n_a x \sin m_b y$ |
| $e_x$ | $= n_{nm} m_b \cos n_a x \sin m_b y$ | $N_{nm} n_a \cos n_a x \sin m_b y$ |
| $e_y$ | $= -N_{nm} n_a \sin n_a x \cos m_b y$ | $N_{nm} m_b \sin n_a x \cos m_b y$ |
| $Y_{nm}$ | $= Y_o \beta_{nm}/k$ | $Y_o k/\beta_{nm}$ |

$$o < x < a, \quad 0 < y < b$$

Note that for both modes:

$$N_{nm} = 4\left[2\epsilon_{on}\epsilon_{om} Y_{nm} ab\,(n_a^2 + m_b^2)\right]^{-\frac{1}{2}}$$

$$\beta_{nm} = \left[k^2 - n_a^2 - m_b^2\right]^{\frac{1}{2}}$$

$$n_a = n\pi/a$$

$$\epsilon_{on} = \begin{cases} 2 & n = 0 \\ 1 & n \neq 0 \end{cases}$$

$$m_b = m\pi/b$$

Table 3.2: Transmission Matrix $[T_{12}]$ from a Rectangular Duct to an Annular Duct

(1) $TM_{nm}$ (rectangular) modes in, $TM_{pq}$ (annular) modes out

$$\left[\Gamma^{ee}_{pq;nm}\right] = \begin{cases} -\frac{b}{4}\frac{z_o}{k}A_{pq}\left(k^2 - \left(\frac{p\pi}{b}\right)^2\right)N_{nm}Y_{nm}m_b\int_{r_b}^{r_a}\sin n_a x R_{pq}(\rho)d\rho \\ -\frac{b}{4}\frac{z_o}{k}A_{pq}\left(\frac{p\pi}{b}\right)N_{nm}Y_{nm}n_a\int_{r_b}^{r_a}\cos n_a x R'_{pq}(\rho)d\rho \\ -\frac{b}{4}\nu_{pq}N_{nm}m_bA_{pq}\int_{r_b}^{r_a}\frac{1}{\rho}\sin n_a x R_{pq}(\rho)d\rho \end{cases}$$

if $p = m$

and $= 0$ if $p \neq m$

$$\text{with} \begin{cases} n = 1, 2, 3, \ldots \\ m = 1, 2, 3, \ldots \end{cases}$$

$$\text{and} \begin{cases} p = 0, 1, 2, \ldots \\ q = 1, 2, 3, \ldots \end{cases}$$

Note: $N_{nm}$, $Y_{nm}$, $M_b$ and $N_a$ are defined in Table 4.1. $\nu_{pq}$, $R_{pq}$, $A_{pq}$ are defined in Equations (3.22), (3.21), (3.35) respectively. $\rho$ and $x$ are related by

$$x = \frac{r_a + r_b}{2} - \rho$$

Table 3.2 continues

(2) $TM_{nm}$ (rectangular) modes in, $TE_{pq}$ (annular) modes out

$$\left[\Gamma^{he}_{pq;nm}\right] = \begin{cases} -\frac{b}{4}\frac{B_{pq}}{z_o k}\left(k^2 - \left(\frac{p\pi}{b}\right)^2\right) N_{nm} n_a \int_{r_b}^{r_a} \cos n_a x R_{pq}(\rho) d\rho \\ -\frac{b}{4}\frac{B_{pq}}{z_o k}\left(\frac{p\pi}{b}\right) N_{nm} m_b \int_{r_b}^{r_a} \sin n_a x R'_{pq}(\rho) d\rho \\ -\frac{b}{4}\nu_{pq} N_{nm} Y_{nm} n_a B_{pq} \int_{r_b}^{r_a} \frac{1}{\rho} \cos n_a x R_{pq}(\rho) d\rho \end{cases}$$

if $p = m$

and $= 0$ if $p \neq m$

$$\text{with} \begin{cases} n = 1, 2, 3, \ldots \\ m = 1, 2, 3, \ldots \end{cases}$$

$$\text{and} \begin{cases} p = 1, 2, 3, \ldots \\ q = 1, 2, 3, \ldots \end{cases}$$

$B_{pq}$ are defined in Equation (3.51). $R_{pq}$,$R'_{pq}$ and $\nu_{pq}$ are defined in the section of $TE$ annular modes.

Table 3.2 continues

(3) $TE_{nm}$ (rectangular) modes in, $TM_{pq}$ (annular) modes out

$$\left[\Gamma^{eh}_{pq;nm}\right] = \begin{cases} \frac{b}{4}\epsilon A_{pq}\frac{z_o}{k}\left(k^2-\left(\frac{p\pi}{b}\right)^2\right)N_{nm}Y_{nm}n_a\int_{r_b}^{r_a}\sin n_a x R_{pq}(\rho)d\rho \\ \frac{b}{4}\epsilon A_{pq}\frac{z_o}{k}\left(\frac{p\pi}{b}\right)N_{nm}Y_{nm}m_b\int_{r_b}^{r_a}\cos n_a x R'_{pq}(\rho)d\rho \\ \frac{b}{4}\epsilon A_{pq}\nu_{pq}N_{nm}n_a\int_{r_b}^{r_a}\frac{1}{\rho}\sin n_a x R_{pq}(\rho)d\rho \end{cases}$$

if $p = m$

and $= 0$ if $p \neq m$

$$\text{with} \begin{cases} n = 0,1,2,3,\ldots \\ m = 0,1,2,3,\ldots \\ n = m = 0 \text{ excepted} \\ p = 0,1,2,3,\ldots \\ q = 1,2,3,\ldots \end{cases}$$

$$\text{and } \epsilon = \begin{cases} 2, & p = m = 0 \\ 1, & p = m \neq 0. \end{cases}$$

$A_{pq}$,$R_{pq}$,$R'_{pq}$ and $\nu_{pq}$ are defined in the section of $TM$ annular modes.

Table 3.2 continues

(4) $TE_{nm}$ (rectangular) modes in, $TE_{pq}$ (annular) modes out

$$\left[\Gamma^{hh}_{pq;nm}\right] = \begin{cases} -\frac{b}{4}\frac{B_{pq}}{z_o k}\left(k^2 - \left(\frac{p\pi}{b}\right)^2\right) N_{nm} m_b \int_{r_b}^{r_a} \cos n_a x R_{pq}(\rho) d\rho \\ -\frac{b}{4}\frac{B_{pq}}{z_o k}\left(\frac{p\pi}{b}\right) N_{nm} n_a \int_{r_b}^{r_a} \sin n_a x R'_{pq}(\rho) d\rho \\ -\frac{b}{4}\nu_{pq} N_{nm} Y_{nm} m_b B_{pq} \int_{r_b}^{r_a} \frac{1}{\rho} \cos n_a x R_{pq}(\rho) d\rho \end{cases}$$

if $p = m$

and $= 0$ if $p \neq m$

$$\text{with} \begin{cases} n = 0, 1, 2, 3, \ldots \\ m = 0, 1, 2, 3, \ldots \\ n = m = 0 \text{ excepted} \\ p = 1, 2, 3, \ldots \\ q = 1, 2, 3, \ldots \end{cases}$$

$B_{pq}$ are defined in Equation (3.51). $R_{pq}$,$R'_{pq}$ and $\nu_{pq}$ are defined in the section of $TE$ annular modes.

# Chapter 4

# Results and Discussion

In this section the fields backscattered from a rectangular, S-shaped duct will be presented in the form of backscatter vs. aspect angle plots. The geometries of an S-shaped duct and a straight duct with rectangular cross-sections are illustrated in Figures 1.1 and 3.1, respectively. The scattering effects included in this analysis are the internal reflection at the duct cavity termination and the external rim diffraction at the duct opening. The structural scattering due the exterior duct surface is not included. The emphasis of this section will be focused on comparing the backscattered fields of an S-shaped duct with those of a straight duct. It is expected that the backscattered patterns will be different because the curvature of an S-shaped duct redistributes the coupled energy in a way that differs from a straight duct. Since both the straight and S-shaped ducts in this analysis are perfectly conducting, none of the energy coupled into the duct is lost. Although the backscattered pattern will change depending on the duct geometry, the average dB level will remain about the same.

First, as a check to the analysis of an S-shaped duct, the backscattered patterns of a 5 section S-shaped duct is obtained in the $x - z$ plane. As shown in Figure 4.1, the lengths of the last 4 sections of this S-shaped duct approach zero. In other words, the geometry of this S-shaped duct is no

different than a straight duct. The height of this duct is 6 inches and the width is 4 inches. At 10 GHz, this translates to 99 propagating modes in the rectangular section and 105 modes in the annular section. The backscattered $E$-theta plot and the $E$-phi plot are shown in Figures 4.1 and 4.2, respectively. The corresponding patterns from a straight duct are shown in Figures 4.3 and 4.4. Comparing the backscattered $E$-theta patterns of Figures 4.1 and 4.3 and comparing the backscattered $E$-phi patterns of Figures 4.2 and 4.4, one finds that they are virtually the same. Consequently, this analysis successfully reduces a more complicated S-shaped duct geometry into a straight duct geometry as far as backscatter patterns are concerned.

Figures 4.5 and 4.6 show the backscattered patterns of an S-shaped duct in the $x - z$ plane. Figure 4.5 also defines the geometry of this S-shaped duct. Comparing these two patterns with those due to a straight duct as shown in Figures 4.3 and 4.4, one finds that the S-shaped duct changes the pattern shape. The coupled energy is redistributed after it radiates back out although the average dB level remains about the same. Moreover, in the $x - z$ plane, the S-shaped duct does not have symmetry in geometry as the straight duct does. Thus the backscattered patterns of the S-shaped duct in this plane are not symmetric, contrary to the patterns due to a straight duct; these effects can be seen from Figures 4.3 to 4.7. The backscattered $E$-theta field of this S-shaped duct, in Figure 4.5, also compares very well with the $TM$ backscatter of a 2-dimensional S-shaped duct as shown in Figure 4.7. This is expected because only the pattern in the principal (horizontal) plane of this 3-dimensional duct is considered. The field patterns due to the other principal (vertical or $y-z$) plane is shown in Figure 4.8. It can be seen that in this plane, the pattern is symmetric because of the symmetry of the structure.

Figures 4.9 to 4.11 show the backscattered patterns of the S-shaped duct

due to different conical pattern cuts. The theta angle is fixed at 10,30 and 45 degrees for Figures 4.9, 4.10 and 4.11 respectively. The phi angle changes from 0 to 360 degrees for each of these figures. It can be seen that the dB levels of these plots are about the same. However, the larger the angle theta, the more the pattern fluctuates. Such characteristics can also be seen in Figure 4.6 which shows nine conical pattern cuts at every 5 degrees from 5 to 45 degrees. Again, this is expected because a small theta angle leads to a small conical pattern variation in circumference. For example, in the extreme case, if theta is zero, the whole conical pattern region will be reduced to a single direction. As a result, a conical pattern with a small theta will not be influenced as much by the radiation from many dominant higher order modes as a conical pattern with a larger theta.

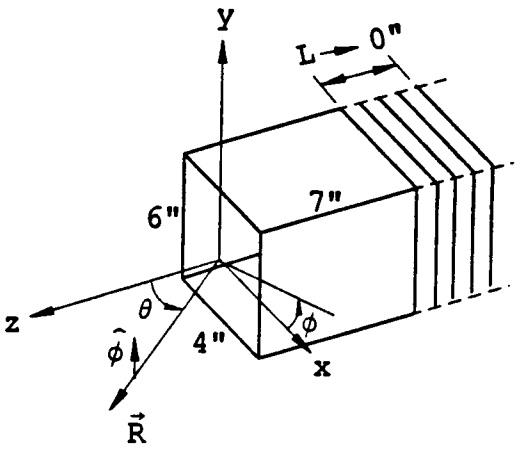


A 5 section S-shaped duct. The lengths of the last 4 sections approach to zero.

## S-Shaped Duct

99 rect modes, 105 annular modes at 10 Ghz

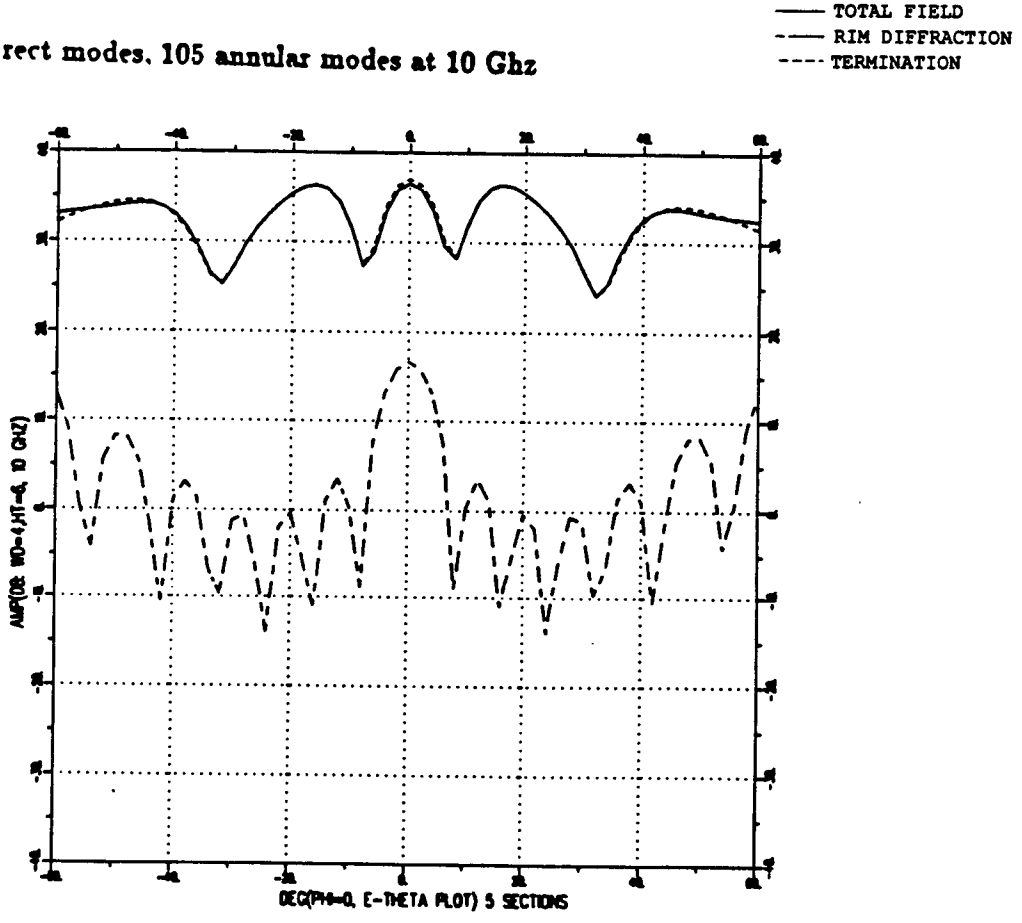


Figure 4.1: Geometry and backscattered $E$-theta plot of an S-shaped duct.

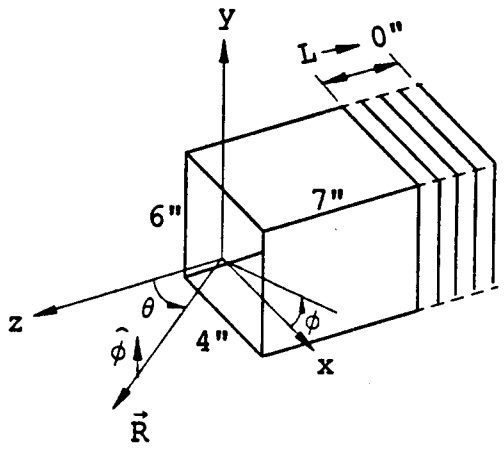


A 5 section S-shaped duct. The lengths of the last 4 sections approach to zero.

## S-Shaped Duct

99 rect modes, 105 annular modes at 10 Ghz

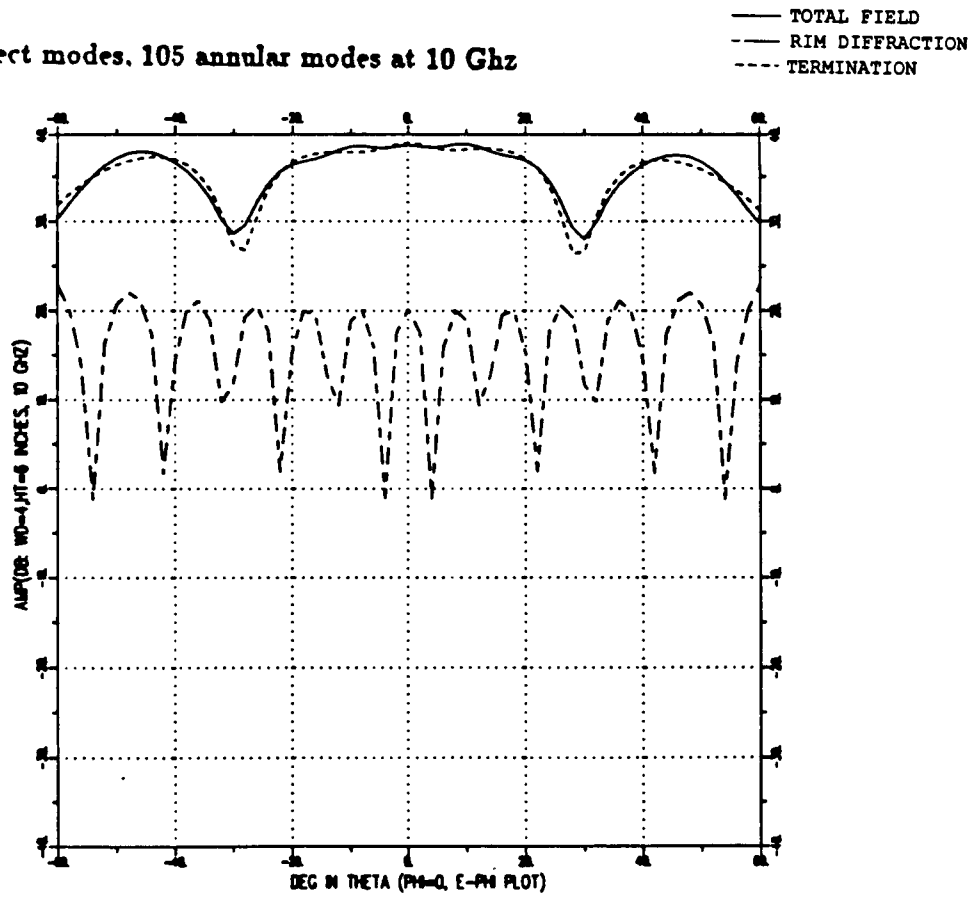


Figure 4.2: Geometry and backscattered $E$-phi plot of an S-shaped duct.

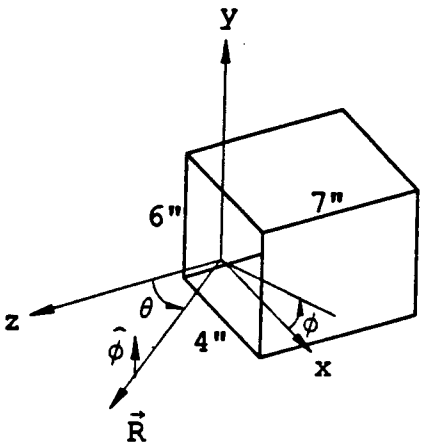


## Rectangular Duct

**Width= 4 inches, Height= 6 inches**

**With 99 propagating Modes at 10 Ghz**

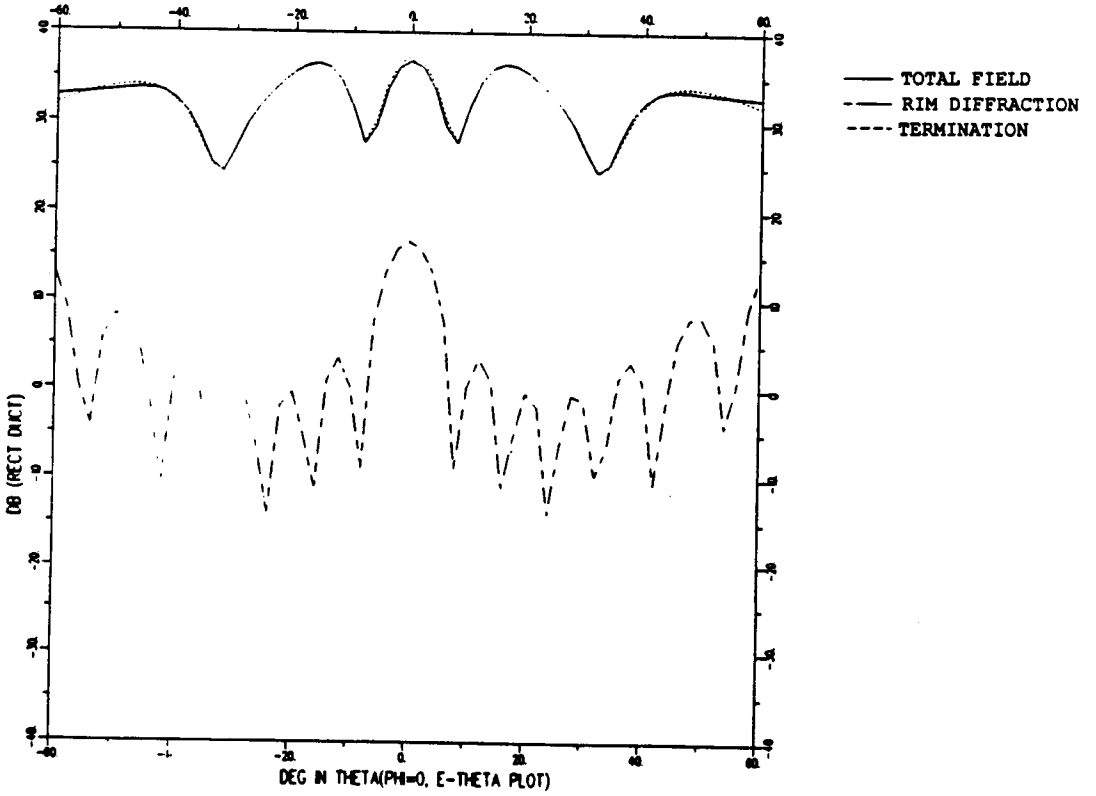


## Backscattered E-Theta Plot

Figure 4.3: Geometry and backscattered $E$-theta plot of a straight duct.

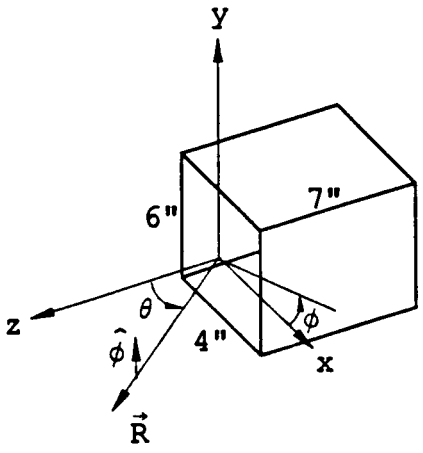


## Rectangular Duct

Width= 4 inches, Height= 6 inches

With 99 propagating Modes at 10 Ghz

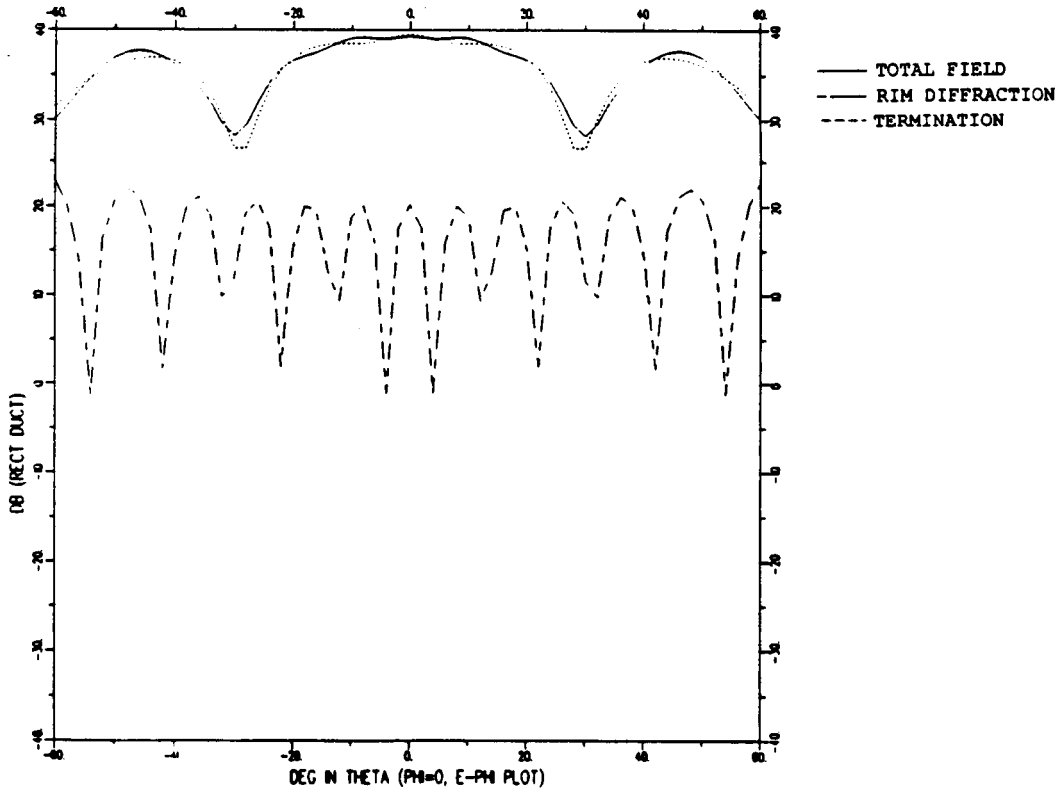


## Backscattered E-Phi Plot

Figure 4.4: Geometry and backscattered $E$-phi plot of straight duct.

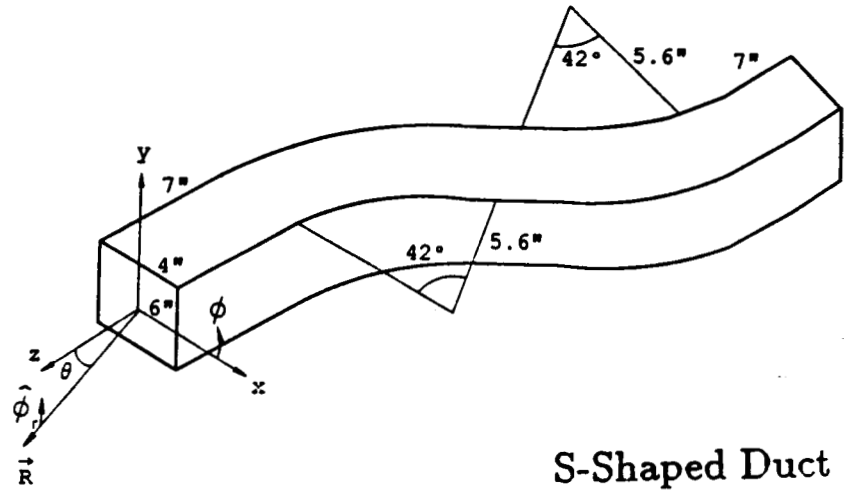


S-Shaped Duct

99 rect modes. 105 annular modes at 10 Ghz

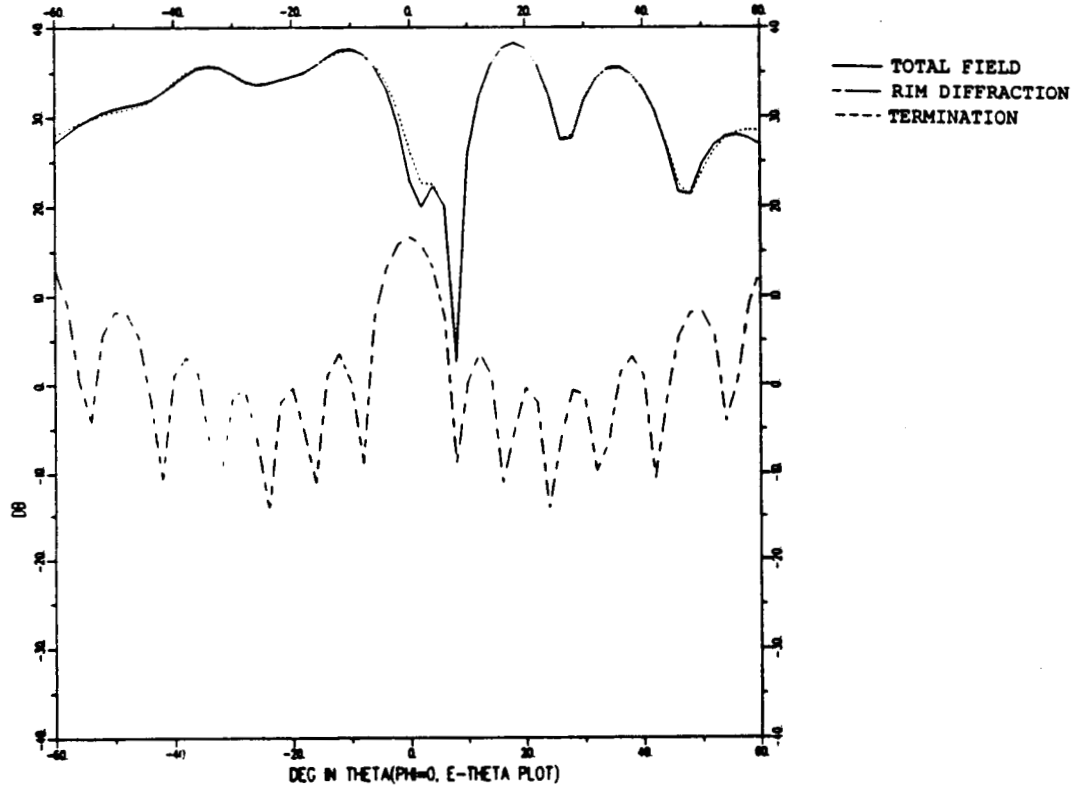


Backscattered E-Theta Plot

Figure 4.5: Geometry and backscattered $E$-theta plot of an S-shaped duct.

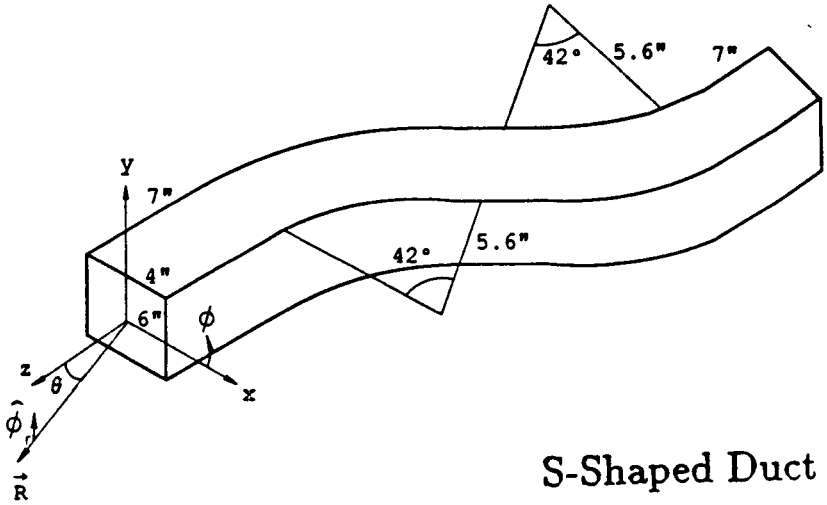


S-Shaped Duct

99 rect modes, 105 annular modes at 10 Ghz

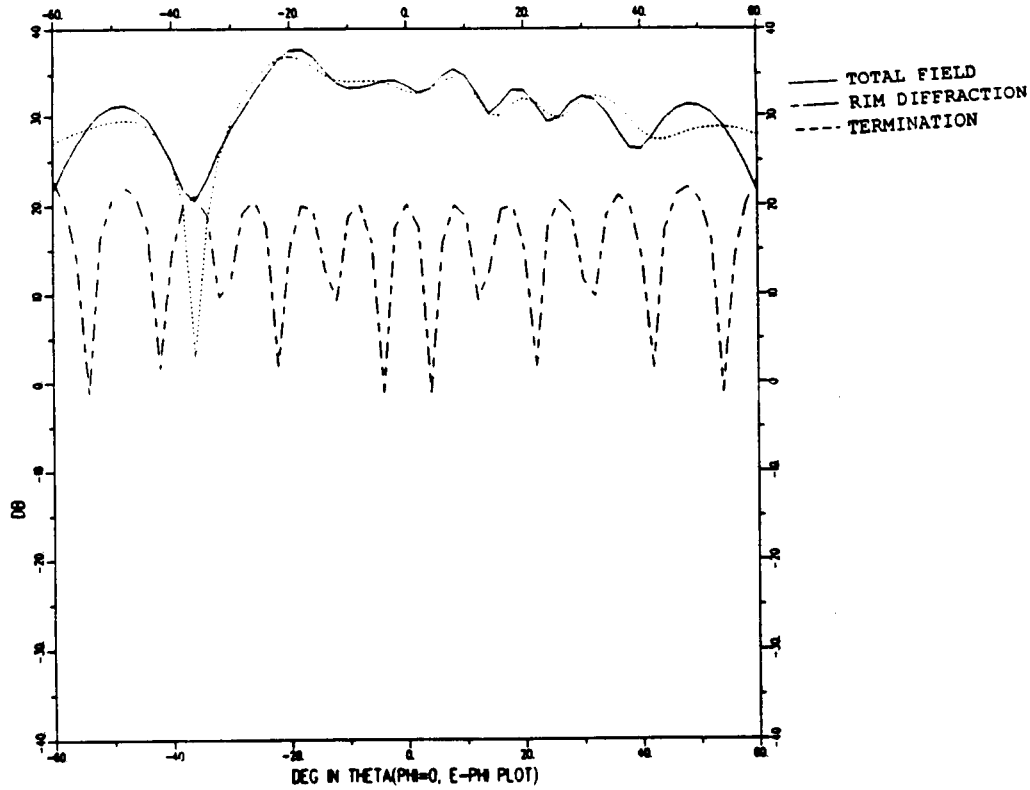


Backscattered E-Phi Plot

Figure 4.6: Geometry and backscattered $E$-phi plot of an S-shaped duct.

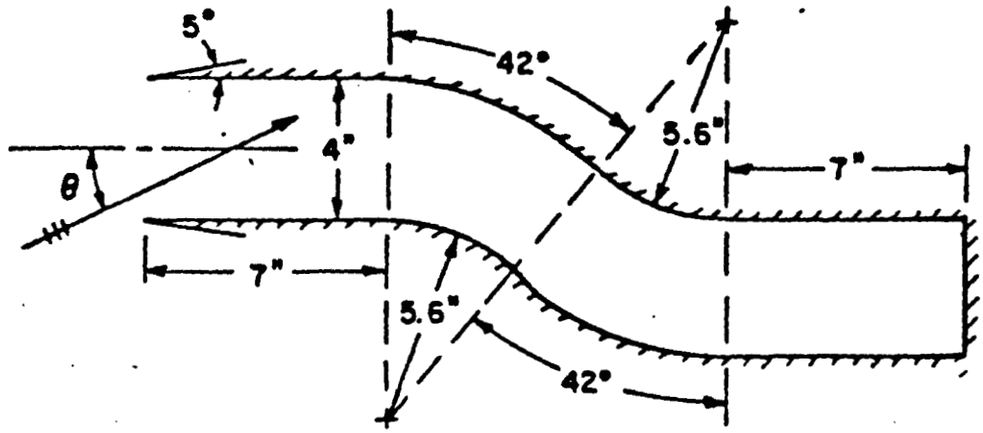


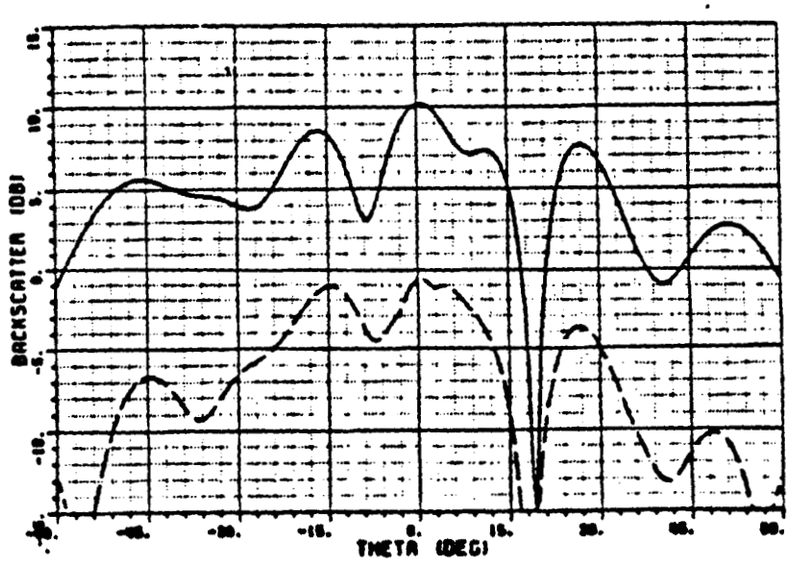


Figure 4.7: Geometry and $TM$ backscatter plot of a 2-dimensional S-shaped duct at 10 Ghz.

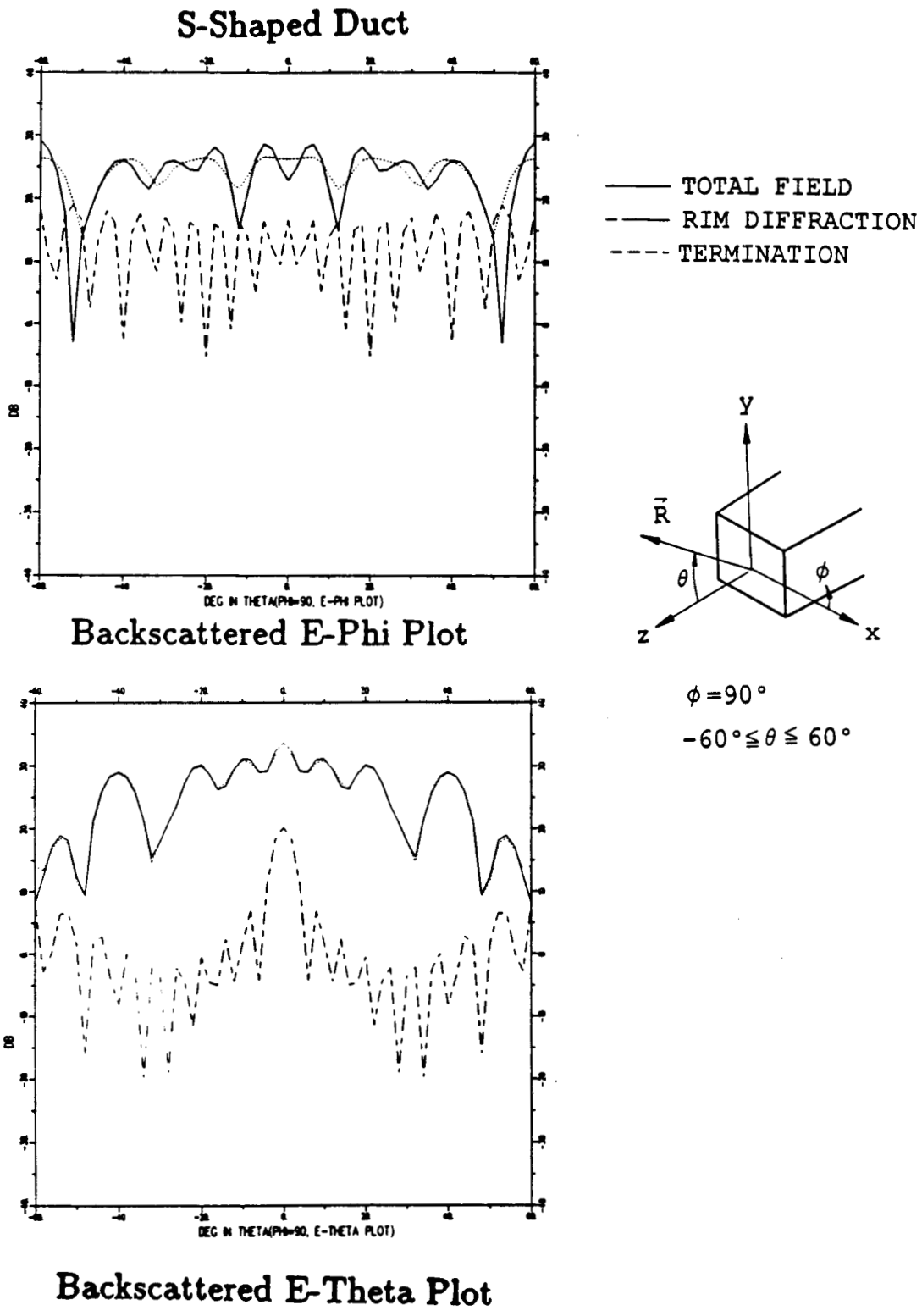


Figure 4.8: Backscattered fields at $y-z$ plane.

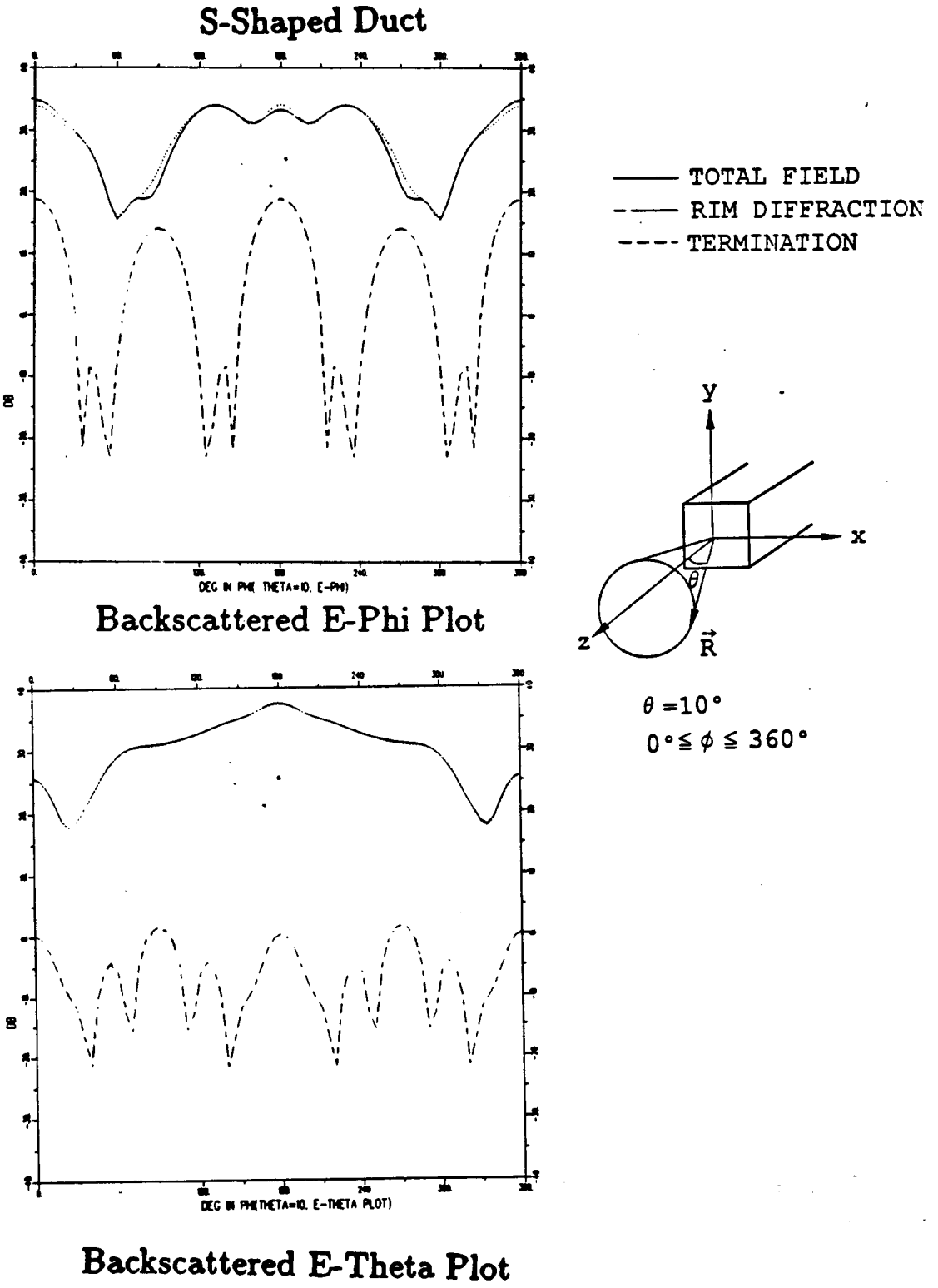


Figure 4.9: Conical pattern cut at $\theta = 10°$.

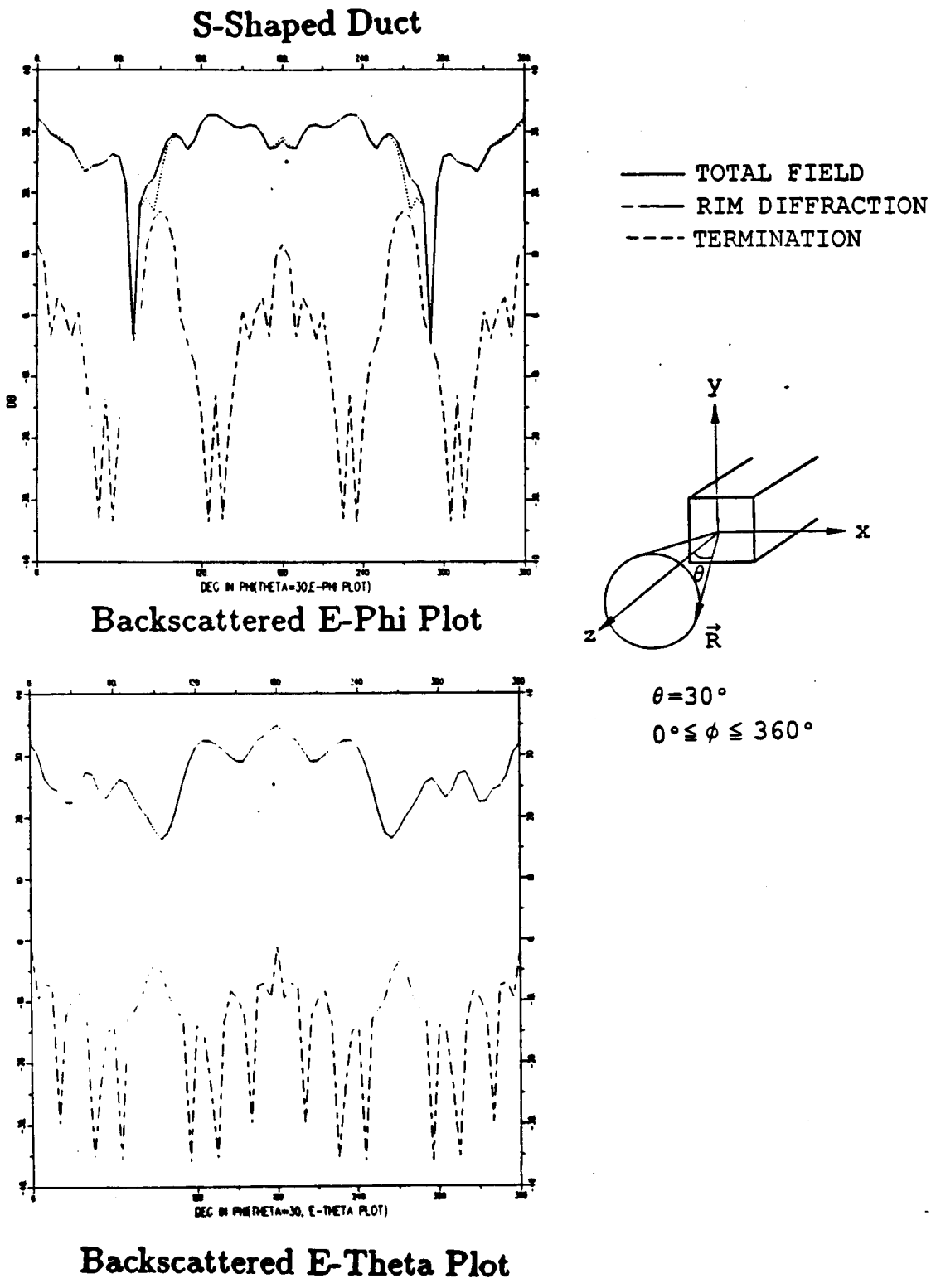


Figure 4.10: Conical pattern cut at $\theta = 30°$.

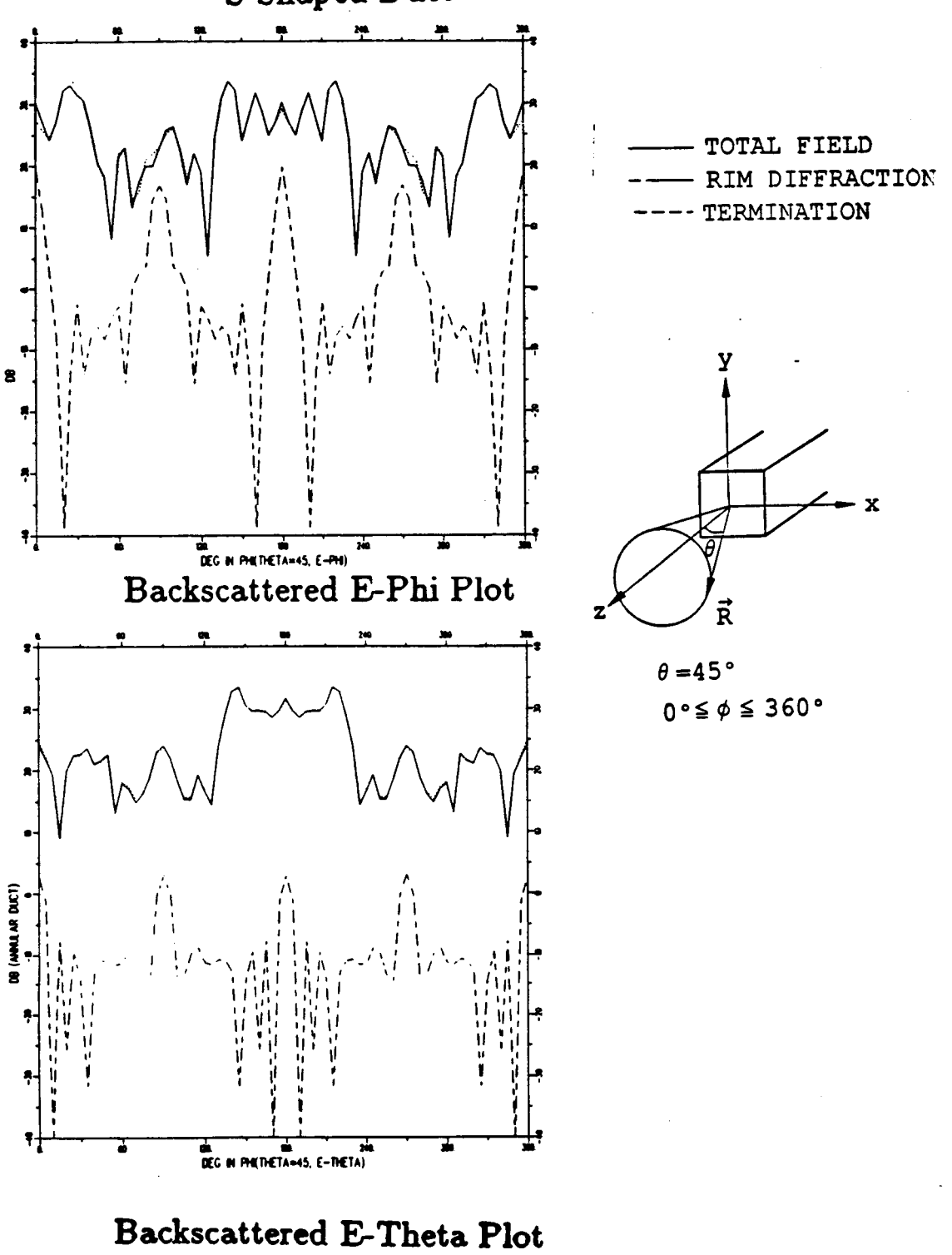


Figure 4.11: Conical pattern cut at $\theta = 45°$.

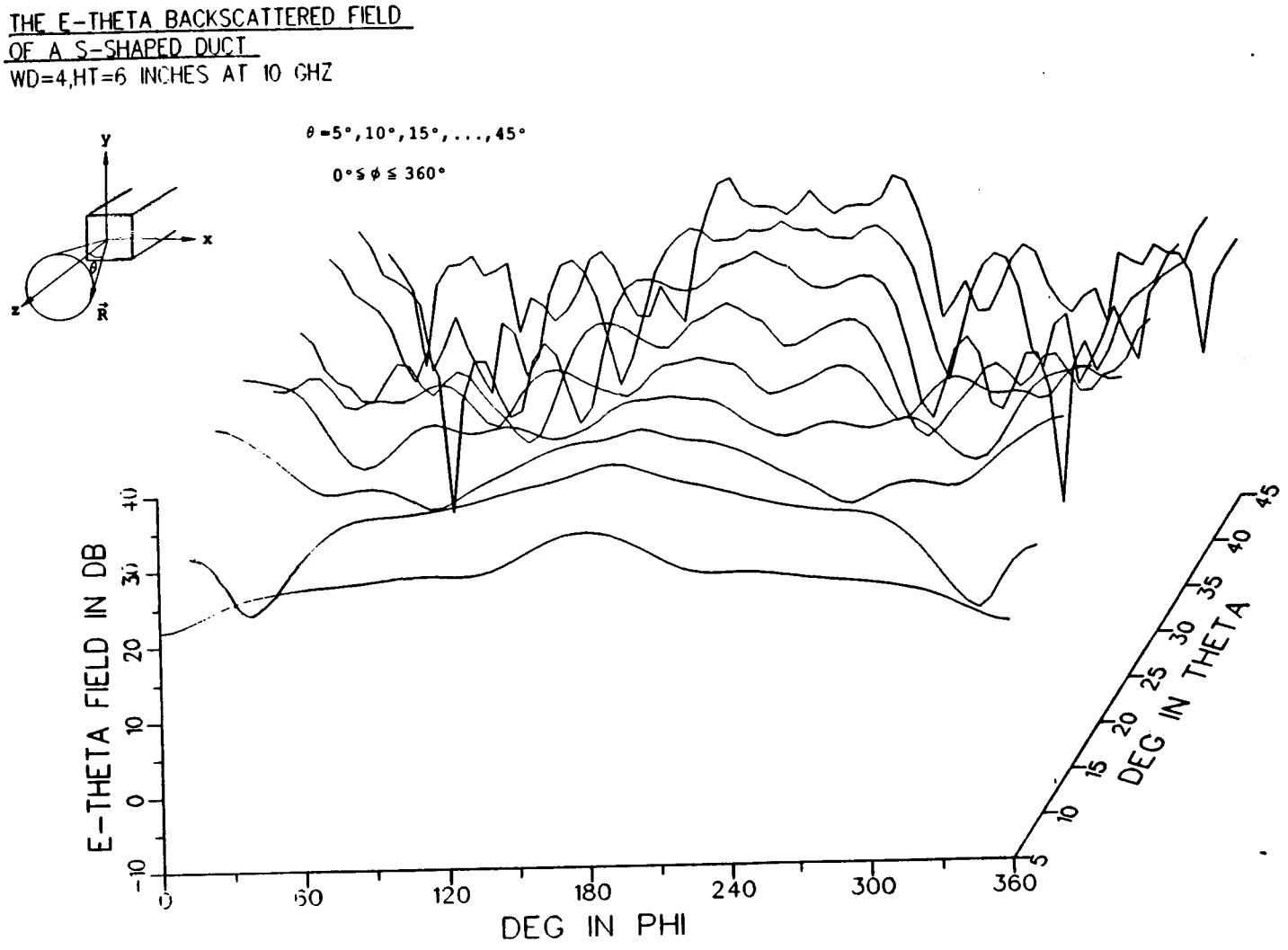


Figure 4.12: Nine conical pattern cuts from $\theta = 5°$ to $\theta = 45°$.

# Bibliography


[1] R.J. Burkholder, C.W. Chuang, P.H. Pathak, "Electromagnetic Fields Backscattered from an S-Shaped Inlet Cavity with an Absorber Coating on its Inner Walls", Final Report 715723-2, The Ohio State University, ElectroScience Laboratory, prepared under Grant NAG 3-476 for NASA- Lewis Research Center, June, 1987.

[2] P.H. Pathak, C.W. Chuang, M.C. Liang, "Inlet Modeling Studies", Technical Report 717674-1, The Ohio State University, ElectroScience Laboratory, prepared under Contract NO. N60530-85-C-0249 for Naval Weapons Center, October 1986.

[3] A. Altintas, P.H. Pathak, W.D. Burnside, "Electromagnetic Scattering from a Class of Open-ended Waveguide Discontinuities", Technical Report 716148-9, The Ohio State University, ElectroScience Laboratory, prepared under Grant NSG 1613 for NASA-Langley Research Center, March, 1986.

[4] P.H. Pathak, A. Altintas, C.W. Chuang and S. Barkeshli," Near Field Scattering by Rectangular and Circular Inlet Configurations with an Impedance Surface Termination", Final Report 715267-1; prepared by th Ohio State University ElectroScience Laboratory for the Naval Weapons Center, China Lake, California on Grant No. N60530-83-M-40RD, July 1984.

[5] R.E. Collin, Foundations for Microwave Engineering, McGraw-Hill, New York, 1966.

[6] R.F. Harrington, Time Harmonic Electromagnetic Fields, McGraw-Hill, New York, 1961.